



# Discovery of novel flavonoid derivatives as potential dual inhibitors against $\alpha$ -glucosidase and $\alpha$ -amylase: virtual screening, synthesis, and biological evaluation

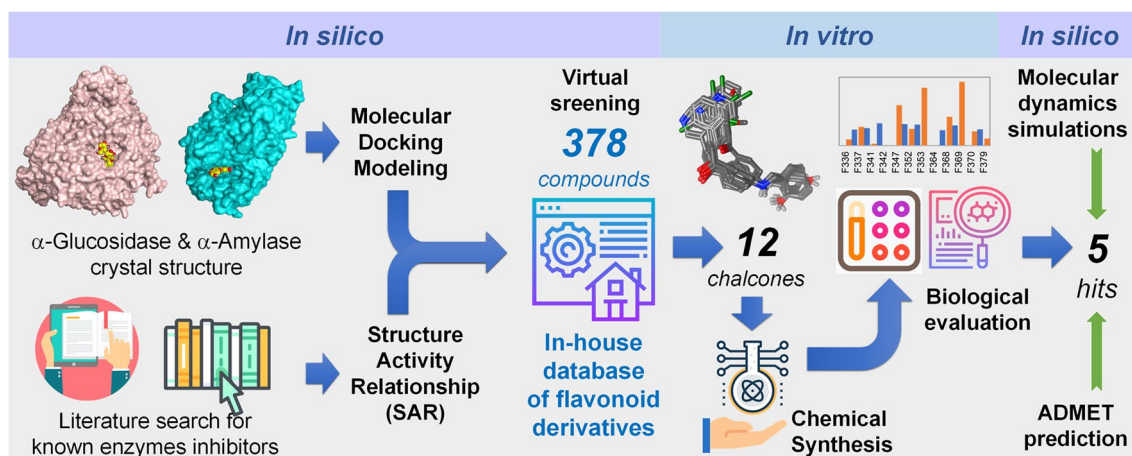
Tan Thanh Mai<sup>1</sup> · Minh-Hoang Phan<sup>1</sup> · Thao Thi Thai<sup>1</sup> · Thua-Phong Lam<sup>1</sup> · Nghia Vo-Trong Lai<sup>1</sup> · Thanh-Thao Nguyen<sup>2</sup> · Thuy-Viet-Phuong Nguyen<sup>1</sup> · Cam-Van Thi Vo<sup>1</sup> · Khac-Minh Thai<sup>1</sup> · Thanh-Dao Tran<sup>1</sup>

Received: 28 January 2023 / Accepted: 17 June 2023  
© The Author(s), under exclusive licence to Springer Nature Switzerland AG 2023

## Abstract

Diabetes mellitus is one of the top ten causes of death worldwide, accounting for 6.7 million deaths in 2021, and is one of the most rapidly growing global health emergencies of this century. Although several classes of therapeutic drugs have been invented and applied in clinical practice, diabetes continues to pose a serious and growing threat to public health and places a tremendous burden on those affected and their families. The strategy of reducing carbohydrate digestibility by inhibiting the activities of  $\alpha$ -glucosidase and  $\alpha$ -amylase is regarded as a promising preventative treatment for type 2 diabetes. In this study, we investigated the dual inhibitory effect against two polysaccharide hydrolytic enzymes of flavonoid derivatives from an in-house chemical database. By combining molecular docking and structure–activity relationship analysis, twelve compounds with docking energies less than or equal to  $-8.0 \text{ kcal mol}^{-1}$  and containing required structural features for dual inhibition of the two enzymes were identified and subjected to chemical synthesis and in vitro evaluation. The obtained results showed that five compounds exhibited dual inhibitory effects on the target enzymes with better  $\text{IC}_{50}$  values than the approved positive control acarbose. Molecular dynamics simulations were performed to elucidate the binding of these flavonoids to the enzymes. The predicted pharmacokinetic and toxicological properties suggest that these compounds are viable for further development as type 2 diabetes drugs.

## Graphical abstract



**Keywords** Chalcone · Dual actions · Diabetes treatment · Molecular docking · Dynamics simulations · Biological evaluation

Extended author information available on the last page of the article

## Introduction

Diabetes mellitus (DM) is a metabolic disease, characterized by a chronically elevated level of blood sugar and caused by an impairment of insulin excretion and/or a decrease in insulin efficiency [1]. According to the report by International Diabetes Federation (IDF) in 2021, about 537 million adults are living with DM and is estimated to rise to 783 million people by the year 2045, making it one of the most prevalent chronic diseases [2]. People with uncontrolled DM are prone to serious implications, including cardiovascular, kidney, eye, and infectious diseases [3]. Type II diabetes (T2DM) is the most common type of DM, accounting for over 90% of all diagnosed DM cases in the world [2, 4]. T2DM is associated with the deficiency of insulin (insulin resistance) and therefore, multiple anti-diabetic agents aiming to increase the level of insulin, enhance the sensitivity of insulin on organs receptors, or decrease the level of blood sugar have been established [5], which could be categorized into subfamilies such as biguanides (metformin), sulfonylureas, meglitinides, thiazolidinediones, glucagon-like-peptide-1 receptor agonist (GLP1-RA), dipeptidyl peptidase IV inhibitors (DPP-4i), sodium-glucose transporter-2 inhibitors (SGLT-2i), and  $\alpha$ -glucosidase inhibitors [1, 5].

A promising approach for the management of T2DM is by inhibiting  $\alpha$ -glucosidase and  $\alpha$ -amylase, the two key enzymes which are responsible for the hydrolyzation and digestion of polysaccharide chains before being absorbed into the bloodstream, thereby reducing the level of blood sugar [6, 7]. Currently available  $\alpha$ -glucosidase inhibitors include acarbose, miglitol, and voglibose, of which the first drug has been launched two decades ago [6]. Different from voglibose and miglitol, acarbose also demonstrates a strong inhibition against  $\alpha$ -amylase, which could explain its strong efficacy in maintaining postprandial blood glucose levels [8]. Moreover,  $\alpha$ -glucosidase inhibitors have also been proven to increase the sensitivity of insulin, thereby releasing the stress on the islet  $\beta$ -cells and slowing down the progression of T2DM [9]. Although having been proven to be well tolerated because of their localized action in the intestine, gastrointestinal side effects such as flatulence, abdominal pain, and diarrhea are the main drawbacks that make this class unpopular in recent years [9]. This raises the need for the exploration and development of new  $\alpha$ -glucosidase and  $\alpha$ -amylase dual-target inhibitors with minimal adverse drug reactions and better efficacy.

$\alpha$ -Amylase (E.C.3.2.1.1) is a digestive enzyme that cleaves starch at  $\alpha$ -1,4-linked glucose molecules to produce a range of shorter polysaccharide chains [10]. In humans,  $\alpha$ -amylase exists in two isoforms, which could be found in saliva and pancreatic fluid [11]. Both isoforms are composed of 496 amino acids and could be divided into three different domains (A, B, and C), with the catalytic triad (Asp197, Glu233, and Asp300) responsible for the cleaving function of the enzymes located in the A domain [12]. On the other hand,  $\alpha$ -glucosidase is a group of small-intestinal brush border-bound hydrolyzing enzymes that cleave disaccharides and oligosaccharides into monosaccharides such as glucose [11]. This group consists of two complexes that work concurrently in the digesting pathway of starch, namely Maltase-glucoamylase (MGAM) and Sucrase-isomaltase (SI) [13], with MGAM (maltase—E.C.3.2.1.20) is the most well-studied enzyme [14]. In humans, the MGAM-containing chain is composed of duplicated catalytic domains, N-terminal MGAM (NtMGAM; residues 1-868) and C-terminal MGAM (CtMGAM; residues 955-1867) [15]. NtMGAM domain has a shallow substrate-binding pocket which allows only 2 sugar subsites whereas the addition of 21 residues in CtMGAM allows this isozyme to cleave a longer chain [14]. In this study, we focused on the NtMGAM, of which, a range of acidic and basic residues (Asp203, Asp327, Asp443, Arg526, Asp571, Asp542, His600) are responsible for the activity of the enzymes [14].

Flavonoid is a ubiquitous phytochemical class that comprises a C6-C3-C6 skeleton and has been widely studied for its broad bioactivity in recent years [16–18]. Moreover, multiple flavonoid structures have been shown to have anti-diabetic properties, via different mechanisms [11, 19, 20]. Therefore, this study aims to assess the dual inhibitory activity of our in-house flavonoid compounds against  $\alpha$ -glucosidase and  $\alpha$ -amylase, using both molecular modeling and experimental approaches. The entire workflow of the screening process for dual inhibitors against  $\alpha$ -amylase and  $\alpha$ -glucosidase has been graphically depicted in Fig. 1. Both structure-based and ligand-based drug design approaches were applied in this work. Using high-quality crystal structures of the two enzymes co-crystallizing with known inhibitors, molecular docking models were constructed for the virtual screening process. The enzyme inhibitors published in the literature allow the establishment of the structure–activity relationships (SARs) to facilitate a more efficient selection of hit compounds for inclusion in chemical synthesis and in vitro experiments. Finally, the flavonoid derivatives identified as dual enzyme inhibitors were further investigated using molecular dynamics (MD) simulations and absorption, distribution, metabolism, excretion, and toxicity (ADMET) evaluation.

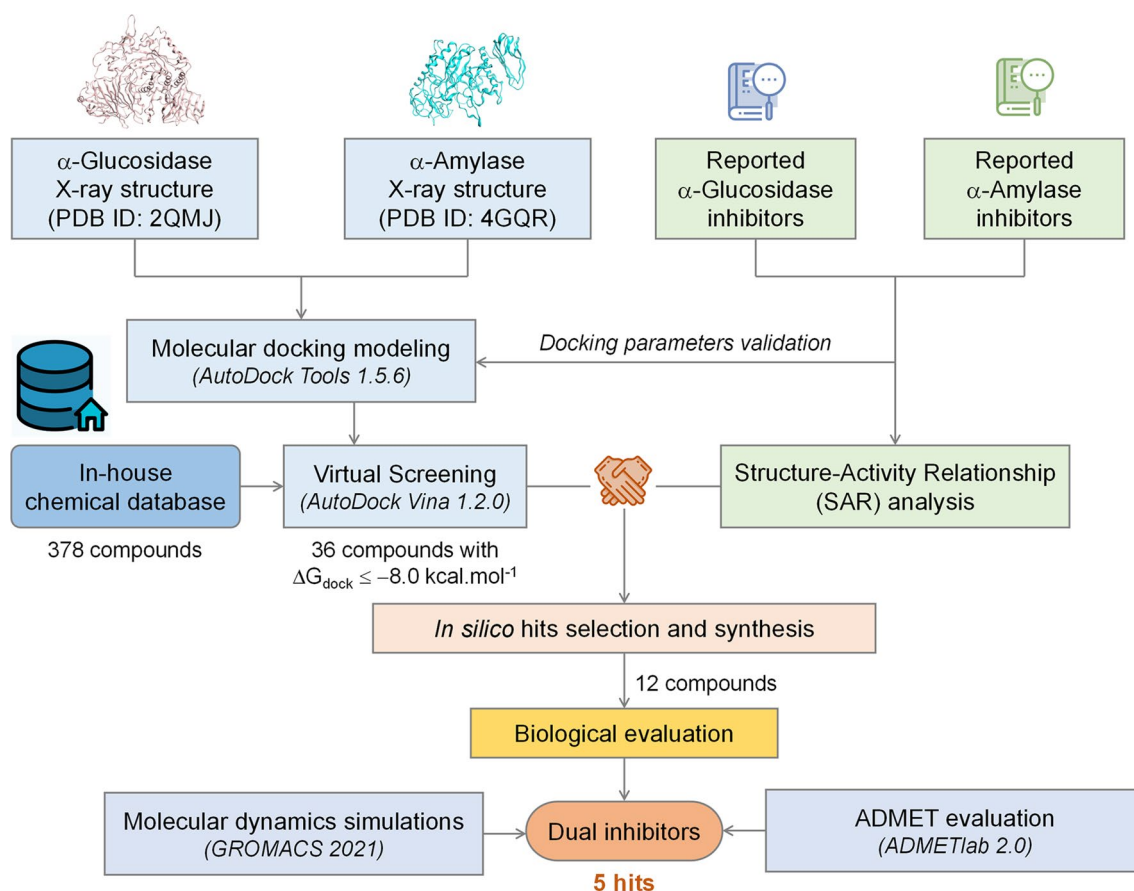


Fig. 1 Schematic representation of the screening process for dual inhibitors against  $\alpha$ -glucosidase and  $\alpha$ -amylase

## Materials and methods

### Molecular docking

The crystal structures of  $\alpha$ -glucosidase and  $\alpha$ -amylase obtained from the Protein Data Bank (PDB) [21] were used to build molecular docking models. Currently, several three-dimensional (3D) structures of  $\alpha$ -glucosidase from various species are available in the PDB. In this current work, the human intestinal  $\alpha$ -glucosidase structure co-crystallized with acarbose imaged by X-ray diffraction method with a resolution of 1.90 Å was used (PDB code: 2QMJ) [14]. Acarbose is one of the well-known  $\alpha$ -glucosidase inhibitors that has been used for the treatment of T2DM [22]. For  $\alpha$ -amylase, the structure of human pancreatic enzyme co-crystallized with myricetin inhibitor captured by X-ray diffraction with 1.20 Å resolution was used (PDB ID: 4GQR) [23]. Myricetin is a member of the flavonoid class of polyphenolic compounds and has been reported to inhibit  $\alpha$ -amylase with an  $IC_{50}$  of 30.2  $\mu$ M [23].

After downloading from the PDB, the enzyme structures in \*.pdb format were processed using the AutoDock Tools 1.5.6rc1 program. First, water molecules and unnecessary

structural components were removed, after which polar hydrogen atoms were added and Kollman charges were assigned to the protein. Finally, the structure of each enzyme was converted into \*.pdbqt format. Molecular docking models were defined by the Grid box function of the AutoDock Tools software. For  $\alpha$ -glucosidase, the size and coordinates of the grid box were determined based on the coordinate of the acarbose and residues in the enzyme catalytic cavity (Asp327, Asp542, His600, Arg526, Asp443, and Asp203). Likewise, the grid box for  $\alpha$ -amylase was established based on the placement of the myricetin and residues in the binding site (Asp197, Glu233, Asp300, Trp59, and Tyr62). The receiver operating characteristic (ROC) curve [24] and the re-docking approach were used to validate the molecular docking models for each enzyme. A docking model is considered reliable if the root-mean-square deviation (RMSD) value between the co-crystallized ligand and its re-docked conformation is less than 2 Å [25]. In the ROC curve assessment method, active and inactive compounds were docked to the enzymes. Active flavonoid compounds were collected from previous studies (detailed in the SAR analysis section). Inactive decoys were generated from active molecules using the DUD-E tool (<http://dude.docking.org>)

[26]. The discriminant ability of molecular docking models was reflected by the ROC curve plotted using the Screening Explorer tool (<http://stats.drugdesign.fr>) [27]. The capability of discrimination between active and inactive compounds of the docking models was assessed using Area Under the ROC curve (AUC-ROC), in which the AUC-ROC value equals 0.5 meaning random discrimination. The higher the AUC-ROC value, the better model's performance [28].

### Database of flavonoid derivatives for virtual screening

In the present work, we used an in-house library containing 378 flavonoid derivatives to investigate the dual inhibition of  $\alpha$ -glucosidase and  $\alpha$ -amylase. The structure in SMILES form and the molecular descriptors according to Lipinski's Rule of Five (Ro5) of the compounds in this chemical library are presented in Table S1. All 378 flavonoid compounds used for virtual screening in this study were designed to satisfy the drug-like properties without more than one violation of Lipinski's Ro5.

The 2D structures of flavonoid derivatives were drawn using ChemDraw 19 software. After that, they were converted into 3D molecules and energy minimized using the Molecular Operating Environment (MOE) software version 2022.10 (<https://www.chemcomp.com>) [29] with a Gradient RMS of 0.0001 kcal mol<sup>-1</sup> Å<sup>2</sup>. During energy minimization, partial charges were calculated and orient –OH groups were optimized. The ligands were then saved in \*.pdb format and converted to \*.pdbqt format using the Open Babel software version 2.4.1 (<https://openbabel.org>) [30]. The ligands were then docked into  $\alpha$ -glucosidase and  $\alpha$ -amylase, respectively, using the AutoDock Vina 1.2.0 software [31] with the previously defined grid box. During the docking process, the exhaustiveness value was set to 8. The investigated compounds were ranked based on their Autodock Vina binding energy ( $\Delta G_{\text{dock}}$ , kcal mol<sup>-1</sup>) and their interactions with the important residues of  $\alpha$ -glucosidase and  $\alpha$ -amylase using the Protein–Ligand Interaction Profiler (PLIP) tools (<https://plip-tool.biotec.tu-dresden.de>) [32].

### Structure–activity relationship analysis of known inhibitors of $\alpha$ -glucosidase and $\alpha$ -amylase

Flavonoid derivatives with  $\alpha$ -glucosidase and  $\alpha$ -amylase inhibitory activities were collected from the literature and used for structure–activity relationship (SAR) analysis. These known inhibitors were also docked into the two enzymes to validate the docking protocols as previously described. Simultaneously, the docking results of these compounds were combined with the SAR analysis to reveal the structural features required for a flavonoid possessing dual inhibitory activity against the enzymes.

In most of the previous reports, the positive control for  $\alpha$ -glucosidase and  $\alpha$ -amylase inhibition assays was acarbose. However, the IC<sub>50</sub> values of acarbose and other inhibitors in different publications are often inconsistent. For the convenience of SAR analysis, the IC<sub>50</sub> values of  $\alpha$ -amylase and  $\alpha$ -glucosidase inhibitor flavonoids were normalized to a standard IC<sub>50</sub> value of acarbose. Particularly, we have collected 51 flavonoid inhibitors of  $\alpha$ -glucosidase from the following original articles [33–38], and [39]. The  $\alpha$ -glucosidase IC<sub>50</sub> values of the compounds were standardized based on the IC<sub>50</sub> value of acarbose at 607  $\mu$ M according to the study of Proença Carina et al. [34]. Similarly, 69 flavonoids inhibiting  $\alpha$ -amylase were collected from publications [40–46], and [17], with the IC<sub>50</sub> value of acarbose used for standardization being 18.08  $\mu$ M according to the research of Saleem Faiza et al. [41]. The lists of known  $\alpha$ -glucosidase and  $\alpha$ -amylase inhibitors are presented in Table S2 and S3, respectively, along with their coding names and standardized IC<sub>50</sub> values. SAR analysis combined with virtual screening by molecular docking will guide the rational selection of flavonoid derivatives for inclusion in the next phase of biological testing.

### Chemicals and instruments

All commercial reagents and solvents were used as received without further purification. Benzaldehyde, 2-chlorobenzaldehyde, 3-chlorobenzaldehyde, 4-chlorobenzaldehyde, 3,4-dichlorobenzaldehyde, 2-chloro-6-fluorobenzaldehyde, 3-pyridinecarboxaldehyde, 4-pyridinecarboxaldehyde, and 2,3-dimethoxybenzaldehyde were purchased from Acros Organics-Thermo Fisher Scientific (Geel-Belgium). The chemicals including 1-(4-((2-hydroxybenzyl)amino)phenyl)ethanone and 1-(4-((4-hydroxybenzyl)amino)phenyl)ethanone were obtained from Medicinal Chemistry's Laboratory, Faculty of Pharmacy, University of Medicine and Pharmacy at Ho Chi Minh city, Vietnam.  $\alpha$ -Glucosidase from *Saccharomyces cerevisiae*, *p*-nitrophenyl- $\alpha$ -D-glucopyranose (*p*-NPG), soluble starch (ACS reagent grade), iodine, and potassium iodide were obtained from Sigma-Aldrich (United States).  $\alpha$ -Amylase from malt was purchased from Himedia (India). Acarbose was procured from Abcam (UK). All the other chemicals were of analytical quality.

The procedures of synthesis were monitored using TLC (Merck, Germany). Nuclear Magnetic Resonance (NMR) spectra were recorded on Bruker (400/500 MHz, Germany) spectrometers. Infrared (IR) spectra were recorded on an IRAffinity-1S Model spectrometer (Shimadzu, Japan) or FTIR-Equinox 55 de Bruker (Germany). UV spectra were recorded on Spectrophotometer UVD-2970 (Labomed, US). Mass spectra were recorded on the MSQ Plus DAD Mass Spectrometer System (Vilber Lourmat, France).

## Synthesis

The synthesis of chalcone derivatives was based on the SAR analysis and molecular docking results, which highlighted specific features for the simultaneous inhibition of  $\alpha$ -glucosidase and  $\alpha$ -amylase. Various chalcone synthesis pathways were available, allowing us to easily modify the scaffold. In terms of A ring substitution, it was observed that the attachment of polar substituents, particularly the amino functional group, enhanced the inhibitory activity of the chalcones. Therefore, we selected the *N*-benzylamino substituent, which could be readily attached to the A ring of the chalcones using substituted acetophenone. In terms of B ring modification, the attachment of functional groups such as hydroxyl, methoxyl, or halogen atoms (Cl or F) was found to further enhance the inhibitory potential. Considering the chemicals available in our laboratory, a series of *N*-benzylaminochalcone derivatives were synthesized for subsequent biological evaluation.

Chalcone derivatives were synthesized via Claisen–Schmidt condensation [47] (Fig. 2). Substituted acetophenone (5 mmol) and aryl-carboxaldehyde derivatives (5 mmol) were dissolved in methanol or ethanol (10 mL) with stirring. Potassium hydroxide (15 mmol) was added slowly in portions to give a dark yellow solution. The resulting solution was stirred at room temperature for 8–12 h, during which chalcone precipitated as the potassium salt. The solution or suspension was poured into cold 0.5 N HCl (10 mL), and further concentrated HCl was added until the solution was acidic. The resulting yellow solid was filtered, washed with water (2 × 20 mL), and recrystallized from a corresponding solvent or purified by flash column chromatography (silica gel, 30% ethyl acetate/hexane) to give the pure product.

### $\alpha$ -Glucosidase inhibition assay

The *in vitro* performance of  $\alpha$ -glucosidase inhibitory activity was based on the protocol used by Zhi-Wei Wang et al. [48] and Graciela Granados-Guzmán et al. [49]. Acarbose was used as the positive control. Accordingly, *p*-NPG was hydrolyzed by the  $\alpha$ -glucosidase to form liberated *p*-nitrophenol (*p*-NP) absorbing 405–415 nm wavelengths. All test samples

were dissolved in DMSO at different concentrations before being used in the assays. The sample solution (10  $\mu$ L) was mixed with 10  $\mu$ L of the  $\alpha$ -glucosidase enzyme (0.5 U mL<sup>-1</sup>) and 150  $\mu$ L of 50 mM phosphate buffer pH 6.8. The mixture was pre-incubated at 37 °C for 60 min. Then, 30  $\mu$ L of 1 mM *p*-NPG solution was added, and the mixture was incubated at 37 °C for another 30 min. The optical absorbance was measured at 405 nm. Each experiment was done in triplicate. The percentage inhibition was calculated according to the formula (1).

$$\text{Inhibitory activity(\%)} = \left( 1 - \frac{\text{Abs}_{\text{sampE}} - \text{Abs}_{\text{sampNE}}}{\text{Abs}_{\text{ctrE}} - \text{Abs}_{\text{ctrNE}}} \right) \times 100 \quad (1)$$

where Abs<sub>sampE</sub> is the absorbance of the sample solution with enzyme, Abs<sub>sampNE</sub> is the absorbance of sample solution without enzyme (replaced by buffer), Abs<sub>ctrE</sub> is the absorbance of the solution containing DMSO replacing the sample and enzyme, and Abs<sub>ctrNE</sub> is the absorbance of the solution containing DMSO replacing the sample without enzyme (replaced by buffer). The IC<sub>50</sub> value was obtained from the linear regression equation when plotting the logarithm of concentration with inhibitory activity (1%).

### $\alpha$ -Amylase inhibition assay

The  $\alpha$ -amylase inhibitory potential was performed *in vitro* by using the iodine starch method. The method was based on the studies of Rie Kusano et al. [50], Zhizhuang Xiao et al. [51], and Maryam Usman Ahmed et al. [52] with slight modification. Acarbose was used as the positive control. Sample or acarbose solutions were prepared by dissolving them in DMSO in various concentrations. The sample solution (25  $\mu$ L) was mixed well with 25  $\mu$ L of 1% soluble starch in distilled water. The mixtures were pre-incubated at 30 °C for 3 min. Then 25  $\mu$ L of enzyme solution (2 U mL<sup>-1</sup> in phosphate buffer pH 6.9) was added to each mixture. Subsequently, they were incubated at 30 °C for 15 min. The reaction was quenched by the addition of 50  $\mu$ L of 1 M HCl, then 125  $\mu$ L of 5 mM iodine solution (5 mM KI and 5 mM iodine). The mixtures were diluted four times and were measured the absorbance at 650 nm. The percentage inhibition was also

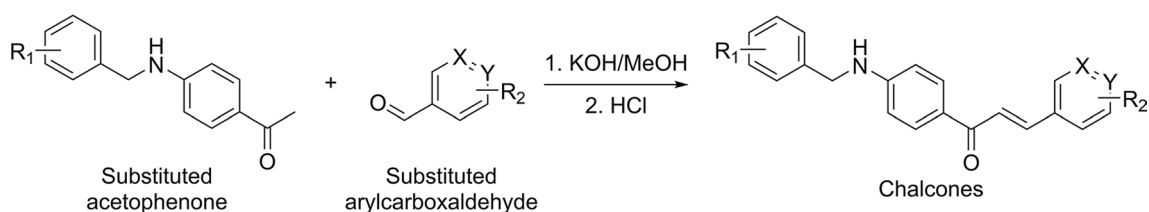


**Fig. 2** Synthesis of chalcone analogs via Claisen-Schmidt condensation

calculated using the formula (1). The  $IC_{50}$  value was derived using the linear regression equation when the logarithm of concentration was plotted against the inhibitory activity ( $I\%$ ).

### Molecular dynamics simulations

To further assess the binding stability of the small molecular inhibitors in the binding sites under a physiological-like environment, molecular dynamics simulations (MDS) were carried out using the GROMACS 2021 program [53]. Briefly, the protein backbone was treated using the built-in CHARMM-27 forcefield [54] and the small-molecule ligands were parameterized using the SwissParam server (<https://www.swissparam.ch>) [55]. The complexes were then put into virtual dodecahedron boxes, in which approximately 29,300 and 22,000 TIP3P solvent molecules were placed for  $\alpha$ -glucosidase and  $\alpha$ -amylase complexes, respectively. The systems were then neutralized by adding  $Na^+$  ions and underwent energy minimization using the steepest descent minimization algorithm with a maximum of 50,000 steps to avoid any geometrical incompatibilities. This is followed by two consecutive 100 ps equilibrium stages namely NVT and NPT equilibrium to stabilize the systems at physiological conditions of 1 bar pressure and 300 K temperature [56]. After achieving equilibrium, the MDS for each complex was produced in 100 ns with a timestep of 2 fs. The MD trajectories were recorded every 0.01 ns and visualized using the VMD [57] and PyMOL program [58]. The built-in

commands of GROMACS 2021 were used to calculate the RMSD (root-mean-square deviation), RMSF (root-mean-square fluctuation),  $R_{\text{gyr}}$  (radius of gyration), and SASA (solvent-accessible surface area) values of the protein backbone or the heavy atoms of the ligands during the MDS. In this study, the hydrogen bonds were determined to occur if the bonding angle between the hydrogen donor (D) and acceptor (A)  $D-H \cdots A$  larger than  $120^\circ$  with the distance between D and A not exceeding  $3.5 \text{ \AA}$  [59].

### ADMET evaluation

ADMET properties of the most potent dual inhibitors on the two enzymes were evaluated using the ADMETlab 2.0 platform (<https://admetmesh.scbdd.com>) [60] to assess their suitability for T2DM drug development. After the SMILES structures are submitted, the online tool will predict their characteristics including physicochemical properties, medicinal chemistry, pharmacokinetics, and toxicity.

## Results

### Molecular docking models for $\alpha$ -glucosidase and $\alpha$ -amylase

From the structure of  $\alpha$ -glucosidase co-crystallized with acarbose collected from the Protein Data Bank (PDB code:

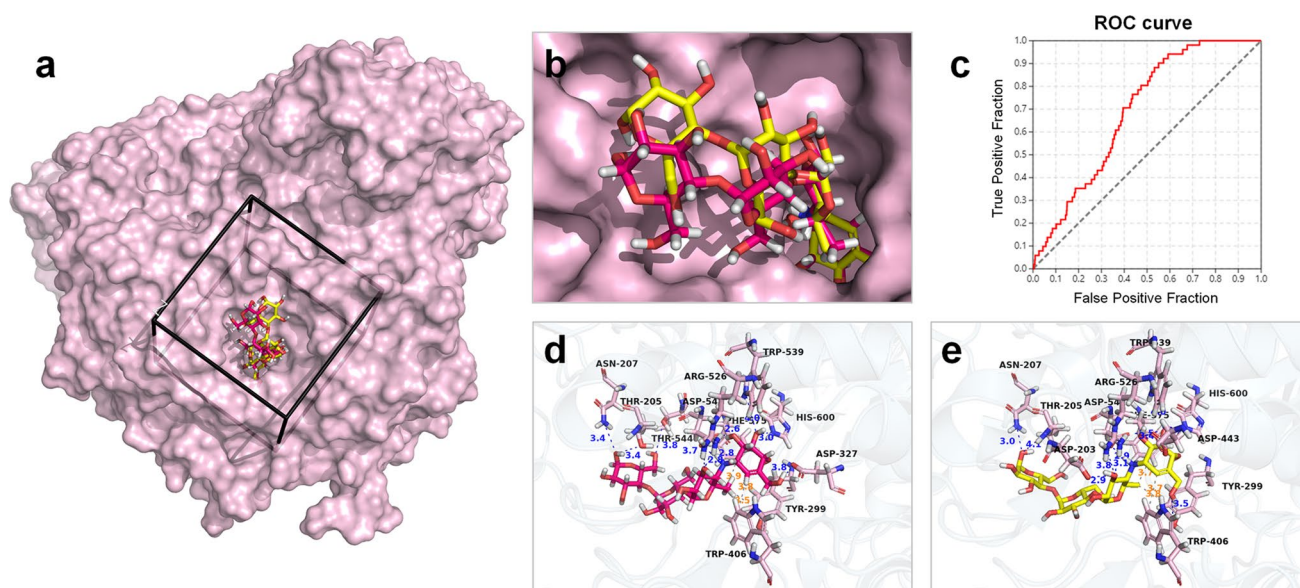


**Fig. 3** Molecular docking model for  $\alpha$ -glucosidase based on the AutoDock package. **a** The 3D structure of  $\alpha$ -glucosidase in the presence of a grid box was determined based on the position of the co-crystallized ligand acarbose. **b** Acarbose in co-crystallized conformation (with carbon atoms in pink) and re-docked conformation

(with yellow carbons). **c** ROC curve obtained from docking process of active and decoy compounds into  $\alpha$ -glucosidase. **d** Interactions of acarbose in co-crystallized conformation and **e** in re-docked conformation with the residues in the active site of the enzyme

2QMJ), an AutoDock grid box was determined from the location of the ligand as shown in Fig. 3a. The grid box had parameters including spacing = 1.0 Å; size<sub>x</sub>, size<sub>y</sub>, and size<sub>z</sub> were 24, 24, and 26, respectively; center<sub>x</sub>, center<sub>y</sub>, and center<sub>z</sub> were -21.957, -3.267, and -7.522, respectively. The model was validated by both re-docking and ROC curves, the results of which are presented in Fig. 3b and c. Using the previously described grid box, acarbose was successfully re-docked into the active site of α-glucosidase and achieved the best docking energy of -8.1 kcal mol<sup>-1</sup> with an RMSD value between the heavy atoms of acarbose in the co-crystallization and re-docked conformation was 1.778 Å (Fig. 3b). Moreover, the docking model is also able to reproduce the main hydrophilic and hydrophobic interactions of acarbose in the binding site of α-glucosidase (Fig. 3d and e). Specifically, the OH groups of acarbose form many hydrogen bonds with the residues such as Thr205, Asn207, Arg526, Trp539, Asp542, and His600. In addition, the hydrophobic interactions between this drug with Tyr299, Trp406, and Phe575 were also re-established. The docking protocol using the above grid box parameter was performed and obtained an AUC-ROC value of 0.690 (>0.5) and a TG value of 0.255 (>0.25), indicating that the docking model could discriminate well between active and inactive compounds (Fig. 3c).

Similarly, a suitable grid box for α-amylase was also identified based on the location of the co-crystallized ligand myricetin. As shown in Fig. 4a, this grid box has the

following parameters: spacing = 1.0 Å; size<sub>x</sub>, size<sub>y</sub>, and size<sub>z</sub> were 22, 20, and 22, respectively; center<sub>x</sub>, center<sub>y</sub>, and center<sub>z</sub> were 12.166, 19.236, and 42.288, respectively. Re-docking of myricetin was given the conformation illustrated in Fig. 4b with an RMSD value compared to the co-crystallization conformation of 1.6797 Å. A ROC curve was plotted from the docking results of the active and decoy datasets to the enzyme (Fig. 4c). The Δ*G*<sub>dock</sub> between myricetin and α-amylase was -7.4 kcal mol<sup>-1</sup>. Myricetin in its re-docked conformation has re-established hydrogen bonds with the residues His101 and Asp197, and hydrophobic interactions with Tyr62 (Fig. 4d and e). The AUC-ROC and TG values obtained were 0.77 (>0.5) and 0.39 (>0.25), respectively. These validation results suggest that the docking models could be used for the next phase of virtual screening to discover novel inhibitors for α-glucosidase and α-amylase.

### SAR analysis of known inhibitors of α-glucosidase and α-amylase

#### SAR of flavonoids inhibiting α-glucosidase

In this SAR analysis, we consider the standardized IC<sub>50</sub> values and Autodock Vina docking energies of 51 known α-glucosidase inhibitors. The detailed data are demonstrated in Table S2. The compounds in this list may have a chalcone, flavone, or flavanone scaffold. The enzyme inhibitory

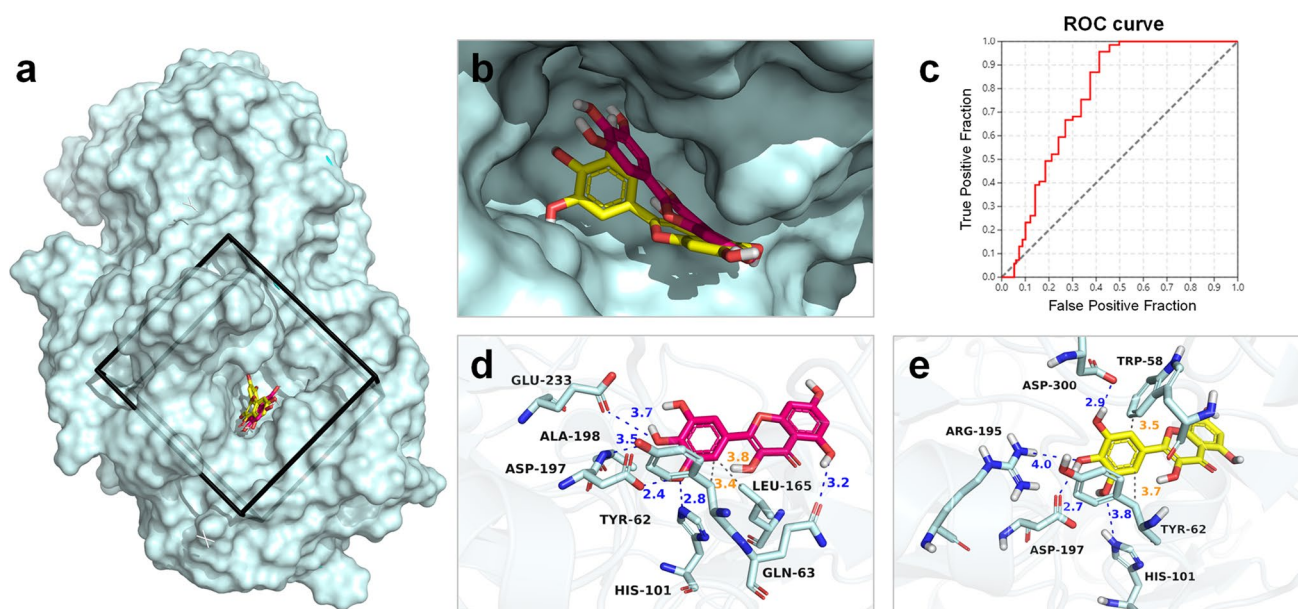
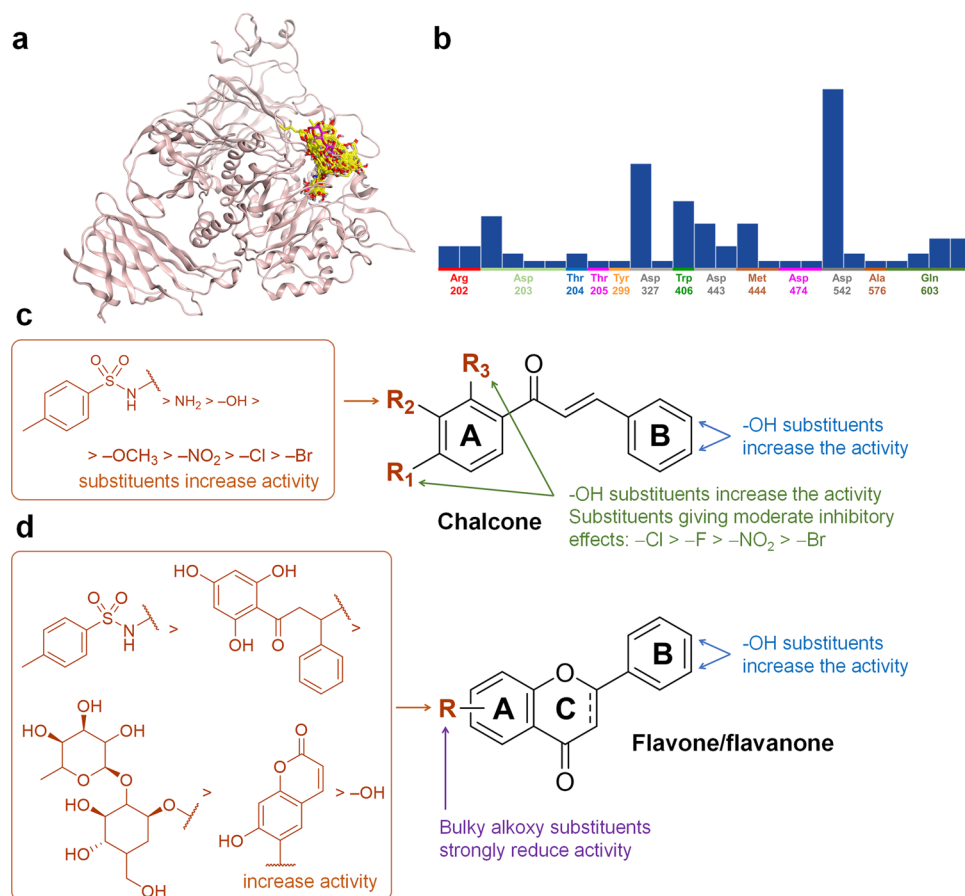


**Fig. 4** Molecular docking model for α-amylase constructed using the AutoDock Tools software. **a** The 3D structure of the enzyme in the presence of a grid box was identified based on the position of the co-crystallized ligand myricetin. **b** Myricetin in co-crystallized conformation (with carbon atoms in pink) and re-docked conformation

(with carbon atoms in yellow). **c** ROC curve obtained from the docking of the true active compounds and corresponding decoy dataset into α-amylase. **d** Interactions of myricetin in co-crystallized conformation and **e** in re-docked conformation with the residues in the active site of α-amylase

**Fig. 5** SAR of  $\alpha$ -glucosidase inhibitors. **a** The best docking conformations of 51 known inhibitors on the enzyme. **b** PLIF analysis of protein–ligand interactions. **c** SAR of  $\alpha$ -glucosidase inhibitors with chalcone scaffold. **d** SAR of  $\alpha$ -glucosidase inhibitors with flavone or flavanone scaffold



activity of flavonoids depends on their substituents as well as the bulkiness of the molecule. Because of the shallow and narrow active site of  $\alpha$ -glucosidase, most flavonoids bind to the gatekeeper residues of the cavity rather than to the catalytic residues located inside the active site (Fig. 5a). By analyzing Protein–Ligand Interaction Fingerprints (PLIF) using MOE software, we found that most of the investigated flavonoids bind to  $\alpha$ -glucosidase by hydrogen bonding with Asp542 and Asp327 by possessing OH groups. In addition, due to the presence of aromatic rings in the flavonoid scaffold, they could also form arene interactions with the aromatic amino acids such as Tyr299 and Trp406 (Fig. 5b). These are four of the key residues in the catalytic cavity of the enzyme. Notably, several inhibitors have given good  $IC_{50}$  values and strong docking energies due to the deep penetration into the active site. They bound well to the enzyme and formed hydrogen bonds with the most important residues, such as Asp203, Asp443, Asp542, and Arg526 in the catalytic cavity.

The chalcone derivatives registered the  $IC_{50}$  values of 9.8 to 409  $\mu$ M and  $\Delta G_{\text{dock}}$  of  $-8.3$  to  $-7.4$  kcal mol $^{-1}$ . To increase the binding capacity to the active site of  $\alpha$ -glucosidase, most studies have focused on developing substituents in the A ring (Fig. 5c). Particularly, the

*N*-substituents toluene sulfonamides result in strong inhibition capacity, especially when the substituent is at the  $R_2$  position (with  $IC_{50} < 10$   $\mu$ M), while the introduction of  $-NH_2$ ,  $-OH$ ,  $-Cl$ ,  $-F$ ,  $-NO_2$ , and  $-Br$  substituents results in moderate inhibitors. On the B ring, the  $-OH$  substituent in the *para* and/or *meta* positions exhibits good inhibitory activity as it could form extra hydrogen bonds with important nucleophilic catalysis residues such as Asp327, Asp443, and Asp542.

On the other hand, the flavone and flavanone derivatives recorded the  $\Delta G_{\text{dock}}$  value varying from  $-9.4$  to  $-7.2$  kcal mol $^{-1}$ . Similar to chalcones, flavanones and flavones have also been focused on expanding the structure in the A ring (Fig. 5d). Adding a sulfonamide group or a chalcone fragment on the A ring gives very strong  $\alpha$ -glucosidase inhibitors ( $IC_{50} < 2$   $\mu$ M) and good docking energies, while adding a sugar fragment or a 7-hydroxy-2*H*-chromene-2-one moiety on the A ring at different positions also establishes good inhibitors compared with acarbose. However, when attaching bulky alkoxy substituents to either the A or B ring, the enzyme inhibitory activity decreased markedly ( $IC_{50} > 2500$   $\mu$ M) and the docking energies were also poor. On the B ring,



most compounds demonstrate that the –OH substituent leads to stronger inhibitors than other substituents.

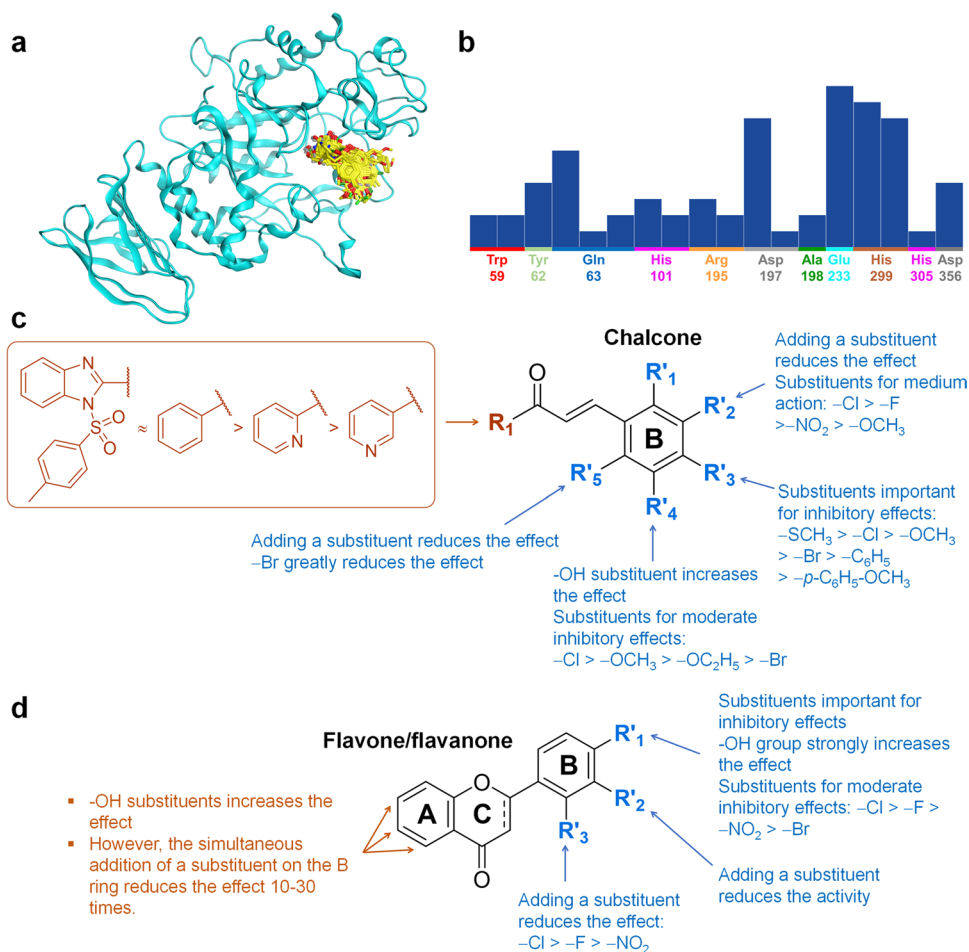
### SAR of flavonoids inhibiting $\alpha$ -amylase

A list of 69 published  $\alpha$ -amylase inhibitors with their  $IC_{50}$  values and Autodock Vina docking energies are presented in Table S3. Most known  $\alpha$ -amylase inhibitors are chalcones. Contrary to the shallow active site of  $\alpha$ -glucosidase, the active site of  $\alpha$ -amylase forms a “V” shape, therefore the ligands could penetrate deeply and fit into the cavity (Fig. 6a). As a result, they could form hydrogen bonds with the three important residues in the catalytic site, including Asp197 and Glu233, hence enhancing the inhibitory activity. Simultaneously, hydrophobic interactions ( $\pi$ - $\pi$ ) were also formed between the aromatic nucleus of the investigated ligand and the hydrophobic residues Tyr59 and Tyr62 (Fig. 6b). The aromatic B ring plays an important role in the inhibition of  $\alpha$ -amylase activity. However, the activity is strong or weak depending on the different substituents attached to this aromatic ring.

Regarding the chalcone structures, the recorded  $IC_{50}$  values ranged from 21 to 40  $\mu$ M while the docking energy

varied between  $-8.5$  and  $-7.1$  kcal mol $^{-1}$ , depending on the variation of substituents attached to both aromatic rings. On the B ring and at the *para* position ( $R'_3$ ), the enzyme inhibitory activity decreased gradually according to the substituents in the following order:  $-SCH_3 > -Cl > -OCH_3 > -Br > -C_6H_5$  (Fig. 6c). The  $-SCH_3$  and  $-OCH_3$  groups play an important role in  $\alpha$ -amylase inhibition as the sulfur or oxygen atom helped direct the binding conformation and formed multiple interactions with residues in the active site. Meanwhile, the phenyl or benzyloxy substituents on this position resulted in a bulkier structure and, therefore, was predicted to cover a larger surface in the binding site with a better  $\Delta G_{dock} < -8$  kcal mol $^{-1}$ , yet the actual  $IC_{50}$  values of these chalcones only indicate moderate inhibition (i.e., compound **BC\_2018\_12** with  $IC_{50} = 34.6$   $\mu$ M and  $\Delta G_{dock} = -8.5$  kcal mol $^{-1}$ ; compound **BC\_2018\_5** with  $IC_{50} = 34.6$   $\mu$ M and  $\Delta G_{dock} = -8.3$  kcal mol $^{-1}$ ). In addition, the halogen or alkyl halogen substituents also demonstrated good  $\Delta G_{dock}$  due to the formation of a hydrophobic interaction ( $\pi$ -alkyl) between the halogen atoms ( $-Cl$ ,  $-F$ ,  $-Br$ ) and the hydrophobic residues Trp59, Trp406, and Phe575 in the active site. Concerning the modification of the  $R_1$  site, the phenyl ring results in the basic chalcone structure while the

**Fig. 6** SAR of  $\alpha$ -amylase inhibitors. **a** The best docking conformations of 69 known inhibitors on the enzyme. **b** PLIF analysis of protein–ligand interactions. **c** SAR of  $\alpha$ -amylase inhibitors with chalcone scaffold. **d** SAR of  $\alpha$ -amylase inhibitors with flavone or flavanone scaffold



replacement of it with another heterocyclic could weaken the inhibitory potency. Particularly, the 2-pyridyl-containing chalcones demonstrate better activity than the 3-pyridyl ones, as the  $\Delta G_{\text{dock}}$  of these chalcones ranged from  $-7.5$  to  $-6.8$  kcal mol $^{-1}$ . Within these heterocyclic-containing chalcones, the introduction of  $-\text{OCH}_3$ ,  $-\text{F}$ ,  $-\text{Cl}$ ,  $-\text{NO}_2$ , or  $-\text{Br}$  substituents on the B ring significantly decreases the inhibitory potency. To be specific, the addition of the  $-\text{Br}$  substituent at any position on this ring negatively impacts the activity, while the addition of the  $-\text{NO}_2$  substituent at the *meta* position (compound **BC\_2021\_16** with  $\text{IC}_{50} = 27.57$   $\mu\text{M}$ , Table S3) demonstrates stronger activity than the *para* position (compound **BC\_2021\_18** with  $\text{IC}_{50} = 51.94$   $\mu\text{M}$ , Table S3). Especially, the replacement of the phenyl ring with [(4-methylphenyl)sulfonyl]-1*H*-benzimidazol-2-yl significantly enhances the inhibitory activity against  $\alpha$ -amylase (i.e., compound **IJC\_2016\_3I** with  $\text{IC}_{50} = 24.86$  and compound **IJC\_2016\_3G** with  $\text{IC}_{50} = 37.29$   $\mu\text{M}$ ). Typically, their  $\Delta G_{\text{dock}}$  ranged from  $-8.4$  to  $-7.4$  kcal mol $^{-1}$ . This is because this substituent helps form extra hydrogen bonds with the three important residues Asp197, Glu233, Asp300 and hydrophobic interactions with Trp59 and Tyr62, revealed by molecular modeling results.

For the flavone scaffold, the introduction of substituents caused the  $\text{IC}_{50}$  values to range from 18.25 to 871  $\mu\text{M}$  and the  $\Delta G_{\text{dock}}$  to range from  $-8.5$  to  $-7.0$  kcal mol $^{-1}$ . Regarding the variation on ring A, the addition of the  $-\text{OH}$  groups simultaneously at three positions 1, 2, and 3, or at 1 and 3 enhances the inhibitory activity, as long as the ring B is kept clean. Replacing the  $-\text{OH}$  group at position 2 with the  $-\text{OCH}_3$  group could lead to a decrease in enzyme inhibitory activity (from 22 to 871  $\mu\text{M}$ ). On the B ring, the introduction of the  $-\text{OH}$  group at the  $R'_1$  position demonstrates the best activity, while that at either  $R'_2$  or  $R'_3$  decreases the activity sharply by 20 times. The activity of flavone derivatives decreased with the addition of  $-\text{Cl}$ ,  $-\text{F}$ ,  $-\text{NO}_2$ , or  $-\text{Br}$  substituents on the B ring (Fig. 6d).

### Structural features required for flavonoid derivatives to have dual inhibitory effects on the two enzymes

By separate SAR analysis on flavonoid compounds with  $\alpha$ -glucosidase or  $\alpha$ -amylase inhibitory activity, several common structural properties were identified. First, the majority of reported enzyme inhibitors belong to the chalcone sub-class of flavonoids. On the A ring, aromatic substituents containing additional polar functional groups are found in both strong inhibitors of  $\alpha$ -glucosidase and  $\alpha$ -amylase. The presence of these substituents enables the inhibitors to form hydrogen bonds and hydrophobic interactions with residues in the catalytic site of the enzymes. On the B ring,  $-\text{OH}$ ,  $-\text{OCH}_3$ , or  $-\text{SCH}_3$  substitutions have

introduced strong inhibitors, but the substitution of the halogen groups (especially the  $-\text{Cl}$  group) also gave potential inhibitors.

### Virtual screening using molecular docking and identification of the top in silico hit compounds

All 378 flavonoid derivatives in our in-house database were successfully docked into the active site of  $\alpha$ -glucosidase and  $\alpha$ -amylase. The compound ID, coupled with their  $\Delta G_{\text{dock-glucosidase}}$  and  $\Delta G_{\text{dock-amylase}}$ , are detailed in Table S4. Regarding the  $\alpha$ -glucosidase docking result, our compounds could bind to  $\alpha$ -glucosidase with Autodock Vina  $\Delta G_{\text{dock}}$  range from  $-9.7$  to  $-5.6$  kcal mol $^{-1}$  as shown in the diagram in Fig. 7a. Most ligands had docking energy of  $-8.0$  to  $-6.0$  kcal mol $^{-1}$ . Of these, 33 investigated compounds have better docking energy than acarbose ( $\Delta G_{\text{dock-glucosidase}} = -8.1$  kcal mol $^{-1}$ ) as shown in Fig. 7b.

At the same time, the flavonoid derivatives in our database could also bind to  $\alpha$ -amylase with a  $\Delta G_{\text{dock}}$  ranging from  $-9.2$  to  $-6.2$  kcal mol $^{-1}$  as shown in the histogram in Fig. 7c. In particular, we have found 215 flavonoids with better docking energies than both myricetin and acarbose (with respective  $\Delta G_{\text{dock-amylase}}$  being  $-7.4$  and  $-6.7$  kcal mol $^{-1}$ ) as illustrated in Fig. 7d. Based on the results of virtual screening using molecular docking, 36 compounds were selected for further analysis because they had docking energies on both enzymes less than or equal to  $-8.0$  kcal mol $^{-1}$  (Fig. 7e). Their chemical structures, docking energies, and interactions with residues in the active sites of  $\alpha$ -glucosidase and  $\alpha$ -amylase are detailed in Table S5.

Of these 36 compounds, together with the previously described SAR analysis, results in the accumulation of 12 compounds which concurrently satisfy our proposed SAR and have a docking affinity lower than  $-8.0$  kcal mol $^{-1}$ . These flavonoid derivatives were submitted to an in vitro biological test to evaluate the inhibitory activity against  $\alpha$ -glucosidase and  $\alpha$ -amylase. Their structure, along with their ID and their binding pattern with  $\alpha$ -glucosidase and  $\alpha$ -amylase, is available in Table 1. As can be seen, all the selected structures compose an *N*-benzylaminochalcone structure. According to the SAR analysis, the introduction of a substituent containing both aromatic rings and polar functional groups (such as 2- or 4-hydroxybenzylamine) to the *para* position of the A ring could help the flavonoids engage deeper in the binding pocket of  $\alpha$ -glucosidase by forming both hydrogen bonds and hydrophobic contacts. Especially for  $\alpha$ -amylase binding, chalcones with large but still flexible substituents such as the hydroxybenzylamine fragment on the A ring will fit into the V-shaped active site of the enzyme. Meanwhile, the B ring was kept clear or attached substituents such as  $-\text{OCH}_3$ ,  $-\text{Cl}$ , or  $-\text{F}$  to enhance the activity against  $\alpha$ -amylase. The presence of

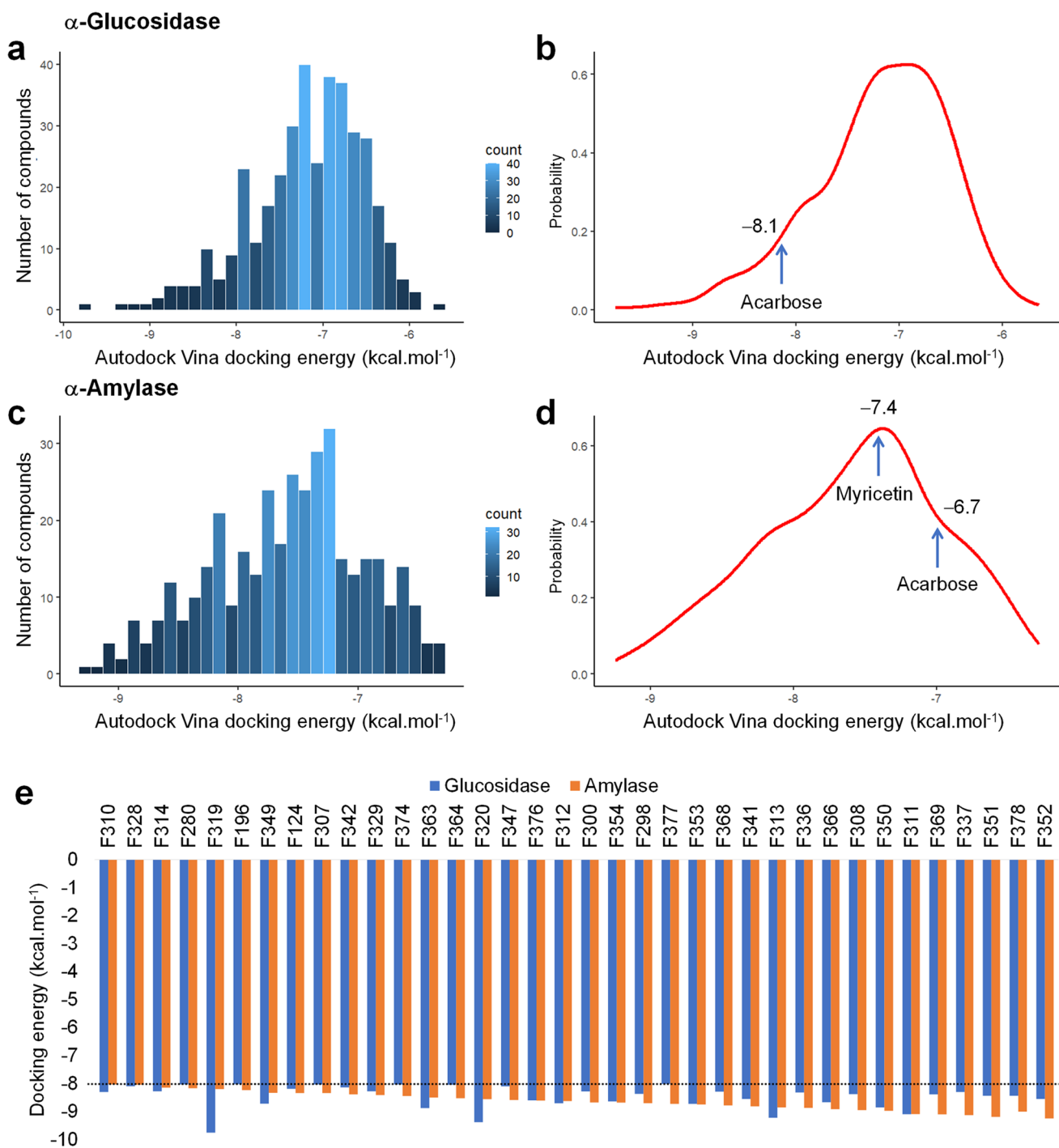


**Fig. 7** Results of virtual screening using molecular docking to identify dual inhibitory flavonoid derivatives for  $\alpha$ -glucosidase and  $\alpha$ -amylase. **a** Histogram and **b** density plot of Autodock Vina docking energies of 378 flavonoid compounds in the in-house database on

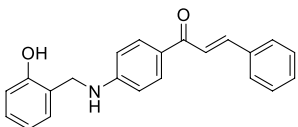
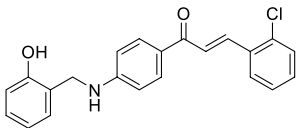
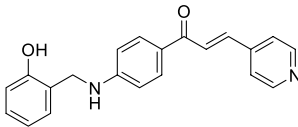
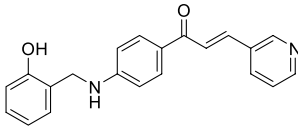
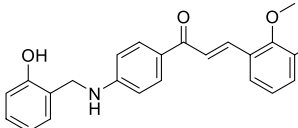
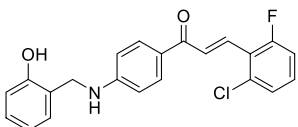
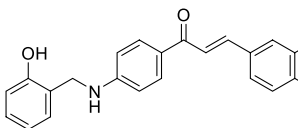
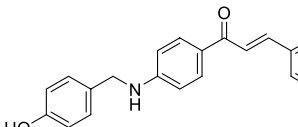
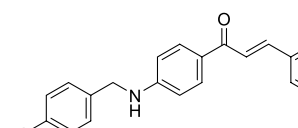
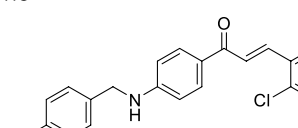
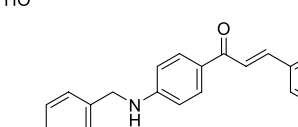
$\alpha$ -glucosidase. **c** Histogram and **d** density plot docking energies of 378 compounds in the database on  $\alpha$ -amylase. **e** The docking energies of the 36 most potential compounds capable of simultaneously binding to the two enzymes with a threshold of less than  $-8.0$  kcal mol<sup>-1</sup>

the  $-OH$  and  $-NH$  groups in the selected flavonoid structures is expected to form multiple hydrogen bonds with the catalytic residues inside the binding cavity of the two enzymes.

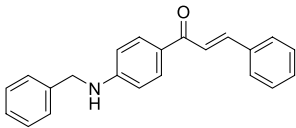
### Chemical synthesis

All flavonoid derivatives demonstrated the potential activities against both  $\alpha$ -glucosidase and  $\alpha$ -amylase by

**Table 1** The top twelve in silico hit compounds selected from virtual screening using molecular docking and SAR analysis

No	Compound ID	2D Structure	Docking into $\alpha$ -glucosidase		Docking into $\alpha$ -amylase	
			$\Delta G_{\text{dock}}$ (kcal mol <sup>-1</sup> )	Interacting residues	$\Delta G_{\text{dock}}$ (kcal mol <sup>-1</sup> )	Interacting residues
1	F336		- 8.3	Asp542, Arg526, Phe450, Trp406	- 8.9	Asp197, Trp58, Trp59, Tyr62
2	F337		- 8.3	Asp542, Arg526, Phe450, Trp406, Phe575	- 9.1	Asp197, Glu233, Trp58, Trp59, Tyr62
3	F341		- 8.5	Asp542, Arg526, Phe450, Trp406, Trp441	- 8.8	Asp197, Glu233, Ala198, Trp58, Trp59, Tyr62
4	F342		- 8.1	Asp542, Arg526, Phe450, Trp406, Trp441, Phe575	- 8.4	Asp197, Glu233, Trp58, Tyr62
5	F347		- 8.1	Asp542, Arg526, Phe450, Trp406	- 8.6	Asp197, Trp58, Trp59, Tyr62
6	F352		- 8.5	Arg526, Asp542, Phe450, Trp441	- 9.2	Asp197, Glu233 Trp58, Trp59, Tyr62
7	F353		- 8.7	Asp542, Arg526, Phe450, Trp406	- 8.7	Asp197, Glu233 Trp58, Tyr62
8	F364		- 8.1	Asp542, Phe575, Phe450	- 8.5	Asp197, Trp58, Tyr62
9	F368		- 8.3	Asp542, Asp327, Phe450, Phe575	- 8.8	Asp197, Trp58, Trp59, Tyr62
10	F369		- 8.4	Asp542, Arg526, Phe450, Trp406	- 9.1	Asp197, Trp58, Tyr62
11	F370		- 8.3	Asp542, Arg526, Phe450, Trp406	- 8.9	Asp197, Trp58, Tyr62, Leu165

**Table 1** (continued)

No	Com- pound ID	2D Structure	Docking into $\alpha$ -glucosidase		Docking into $\alpha$ -amylase	
			$\Delta G_{\text{dock}}$ (kcal mol <sup>-1</sup> )	Interacting residues	$\Delta G_{\text{dock}}$ (kcal mol <sup>-1</sup> )	Interacting residues
12	F378		-8.0	Asp542, Phe450, Phe575	-8.2	Asp197, Trp59, Tyr62

in silico screening are chalcone-structural compounds, including **F336**, **F337**, **F341**, **F342**, **F347**, **F352**, **F353**, **F364**, **F368**, **F369**, **F370**, and **F378**. They were synthesized with high purity via Claisen–Schmidt condensation (over 96%, performed by HPLC). This process afforded the desired chalcones with an average yield of 45–85%. The <sup>1</sup>H-NMR spectra of synthesized chalcones displayed two doublets at  $\delta$  6.2–8.0 ppm with characteristic coupling constant ( $J$ ) of 15–16 Hz, which confirms the formation of chalcones (possessing an  $\alpha,\beta$ -unsaturated carbonyl ketone). This higher coupling constant value indicates all synthetic compounds were geometrically pure and were exclusively trans ( $E$ ) isomers [61]. The information from <sup>1</sup>H-NMR, <sup>13</sup>C-NMR, HPLC, and MS of all synthesized chalcones was attached to the Supplementary Information.

## Biological assays

A preliminary assessment of the inhibitory activity of the screened compounds was conducted using a uniform concentration of 1 mM. Repeating previous studies, acarbose exhibits dual inhibition of  $\alpha$ -glucosidase and  $\alpha$ -amylase. As can be seen in Fig. 8a, regarding the  $\alpha$ -glucosidase inhibition, eight over twelve compounds were able to inhibit the enzyme all over 60% and more strongly than acarbose (56,52%). The inhibitory activity of **F336**, **F347**, **F364**, and **F370** could not be determined because the reaction mixtures were cloudy. At lower concentrations, the IC<sub>50</sub> values of all 12 compounds against  $\alpha$ -glucosidase were determined and detailed in Table 2.

For the  $\alpha$ -amylase inhibition assay, the inhibitory activities of the flavonoid compounds and acarbose at 1 mM concentration vary significantly, yet stand far below 50% (Fig. 8b). Therefore, a higher concentration of substances

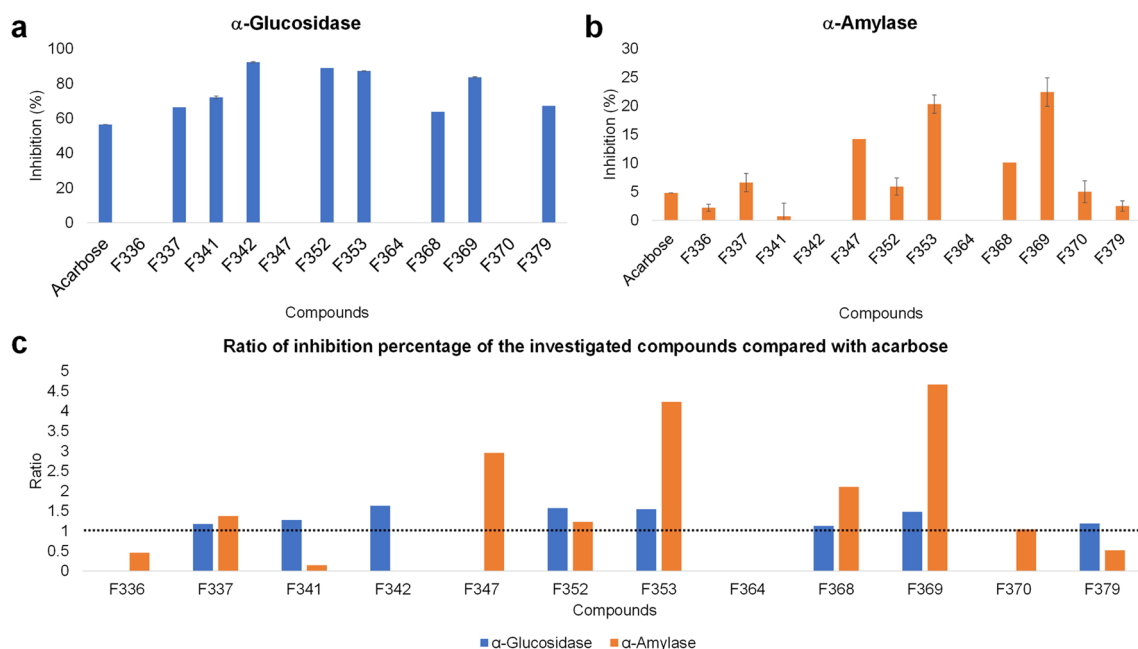


**Fig. 8** The inhibitory activity of the twelve flavonoid derivatives against **a**  $\alpha$ -glucosidase and **b**  $\alpha$ -amylase. **c** Ratio of inhibition percentage of the investigated compounds compared with acarbose

**Table 2** The inhibitory activities of the top twelve flavonoid derivatives against  $\alpha$ -glucosidase and  $\alpha$ -amylase

Compound	$\alpha$ -Glucosidase		$\alpha$ -Amylase	
	I% <sup>a</sup>	IC <sub>50</sub> ( $\mu$ M)	I% <sup>b</sup>	IC <sub>50</sub> (mM)
F336	79.64 $\pm$ 0.42	65.91 $\pm$ 4.16	2.2 $\pm$ 1.6	n.d
F337	54.98 $\pm$ 0.85	251.73 $\pm$ 6.32	6.6 $\pm$ 2.3	7.58 $\pm$ 0.10
F341	64.15 $\pm$ 0.79	131.97 $\pm$ 8.08	0.7 $\pm$ 2.4	n.d
F342	60.75 $\pm$ 0.64	148.04 $\pm$ 7.03	Negative	n.d
F347	63.52 $\pm$ 0.16	291.40 $\pm$ 1.77	14.2 $\pm$ 1.5	5.67 $\pm$ 0.14
F352	70.77 $\pm$ 0.15	158.24 $\pm$ 4.13	5.9 $\pm$ 1.6	n.d
F353	78.73 $\pm$ 0.21	34.28 $\pm$ 0.62	20.3 $\pm$ 1.3	n.d
F364	54.39 $\pm$ 0.21	554.25 $\pm$ 7.46	Negative	n.d
F368	52.82 $\pm$ 0.39	358.89 $\pm$ 10.04	10.1 $\pm$ 2.5	n.d
F369	45.11 $\pm$ 0.26	303.58 $\pm$ 3.63	22.4 $\pm$ 1.9	2.55 $\pm$ 0.14
F370	59.59 $\pm$ 0.72	380.92 $\pm$ 13.15	5.0 $\pm$ 0.9	15.06 $\pm$ 0.31
F378	54.03 $\pm$ 0.29	294.25 $\pm$ 7.32	2.5 $\pm$ 1.7	8.74 $\pm$ 0.55
Acarbose	45.14 $\pm$ 0.36	609.67 $\pm$ 13.61	4.8 $\pm$ 0.6	35.60 $\pm$ 0.56

n.d. not detected due to the poor solubility of the ligands

<sup>a</sup>Inhibition percentage determined at 0.5 mM concentration of the investigated compounds

<sup>b</sup>Inhibition percentage determined at 1.0 mM concentration of the investigated compounds

was used in this experiment. The detailed inhibitory activity, regarding the inhibitory percentage and IC<sub>50</sub> value of the tested compounds, is shown in Table 2. Based on the ratio of I% of the investigated flavonoids to acarbose, Fig. 8c shows that **F337**, **F352**, **F353**, **F368**, and **F369** have a better dual inhibitory effect on the two enzymes than acarbose.

### $\alpha$ -Glucosidase inhibitory activity

In Table 2, for ease of comparison, we present the percentage of  $\alpha$ -glucosidase inhibition at 0.5 mM because the twelve compounds were all soluble at this concentration. In this assay, the obtained IC<sub>50</sub> value of acarbose was 609.67 $\pm$ 13.61  $\mu$ M, which was comparable to the findings of Nasli Esfahani et al. [62] or Zawawi et al. [63]. Surprisingly, all the 12 tested compounds were able to inhibit  $\alpha$ -glucosidase stronger than acarbose. Most compounds have higher I% values than the positive control compound. Additionally, their IC<sub>50</sub> values range from 34.28 to at most 554.25  $\mu$ M, compared to only 609.67  $\mu$ M for acarbose. These results indicate that the combination of SAR analysis and molecular modeling was able to produce outstanding results.

### $\alpha$ -Amylase inhibitory activity

In terms of  $\alpha$ -amylase inhibition, the reaction mixtures of the majority of the tested compounds were turbid when

performed at concentrations greater than 20 mM. Therefore, there were only five compounds with retrievable IC<sub>50</sub> values. However, the results are also very promising as all five compounds (**F341**, **F347**, **F369**, **F370**, and **F378**) could inhibit the  $\alpha$ -amylase at much lower IC<sub>50</sub> values than acarbose, with the most potent compound being **F369** (IC<sub>50</sub>=2.55 $\pm$ 0.14 mM).

In summary, our computational approaches, together with the SAR analysis, were able to retrieve outstanding candidates for the treatment of T2DM. From the present data, we have identified 5 novel flavonoid derivatives with dual inhibitory effects against  $\alpha$ -glucosidase and  $\alpha$ -amylase with determined IC<sub>50</sub> values, including the compound **F337**, **F347**, **F369**, **F370**, and **F378**. These hit compounds inhibit  $\alpha$ -glucosidase approximately 2 times more potently than acarbose and  $\alpha$ -amylase approximately 2–14 times more potently than acarbose. They were subjected to MDS to simulate the interaction between their small molecular structure and the enzymes thereby comprehending the mechanism of inhibition of these compounds.

### Molecular dynamics simulations (MDS)

The semi-flexible docking algorithm of the Autodock Vina algorithm only treats ligands as flexible, while the protein sidechains are kept rigid. Although a fully flexible algorithm has also been developed in this docking program, its flexibility still limits to certain residues surrounding the ligands. Therefore, a series of 100 ns (ns) MDS was conducted to gain insights into the inhibitory mechanism of our investigated compounds.

### Stability of protein–ligand complexes

The stability of the complexes was evaluated using the RMSD, SASA, and R<sub>gyr</sub> values of the protein backbone during the MDS period. The mean values of these values during the MDS trajectories are shown in Table 3.

For comparison purposes, the binding states of acarbose inside the binding cavities of the two enzymes of interest were also extracted. The initial stage of acarbose inside the binding pocket of  $\alpha$ -amylase was created using the previously described docking protocol with the acarbose structure extracted from the  $\alpha$ -glucosidase co-crystallized complex used in our study. The initial stage was assessed to be comparable to the crystal structure of  $\alpha$ -amylase-acarbose available on the PDB (PDB ID: 1XCX) [12] before being undergone a 100 ns MDS. The binding conformations of the acarbose in complex with  $\alpha$ -glucosidase and  $\alpha$ -amylase are available in Fig. S1.

Regarding the  $\alpha$ -glucosidase complexes, as can be seen in Table 3, there was no significant difference between the flavonoid-protein complexes and the acarbose-protein

**Table 3** Stability parameters of the protein backbone during the MD simulations

Protein backbone	Complexes of $\alpha$ -glucosidase			Complexes of $\alpha$ -amylase		
	RMSD (nm)	SASA (nm <sup>2</sup> )	R <sub>gyr</sub> (nm)	RMSD (nm)	SASA (nm <sup>2</sup> )	R <sub>gyr</sub> (nm)
Acarbose	0.149 ± 0.015	455.459 ± 2.125	2.434 ± 0.006	0.161 ± 0.019	270.768 ± 1.586	2.101 ± 0.007
F337	0.140 ± 0.009	455.903 ± 2.018	2.433 ± 0.006	0.164 ± 0.024	270.971 ± 1.690	2.121 ± 0.010
F347	0.157 ± 0.017	456.482 ± 2.021	2.435 ± 0.007	0.149 ± 0.017	271.488 ± 1.790	2.099 ± 0.012
F369	0.139 ± 0.008	455.047 ± 1.938	2.430 ± 0.007	0.182 ± 0.025	269.589 ± 1.491	2.126 ± 0.013
F370	0.143 ± 0.008	454.483 ± 2.076	2.437 ± 0.007	0.185 ± 0.020	272.538 ± 1.610	2.122 ± 0.011
F378	0.147 ± 0.014	456.796 ± 2.065	2.438 ± 0.006	0.148 ± 0.031	270.019 ± 1.549	2.101 ± 0.008

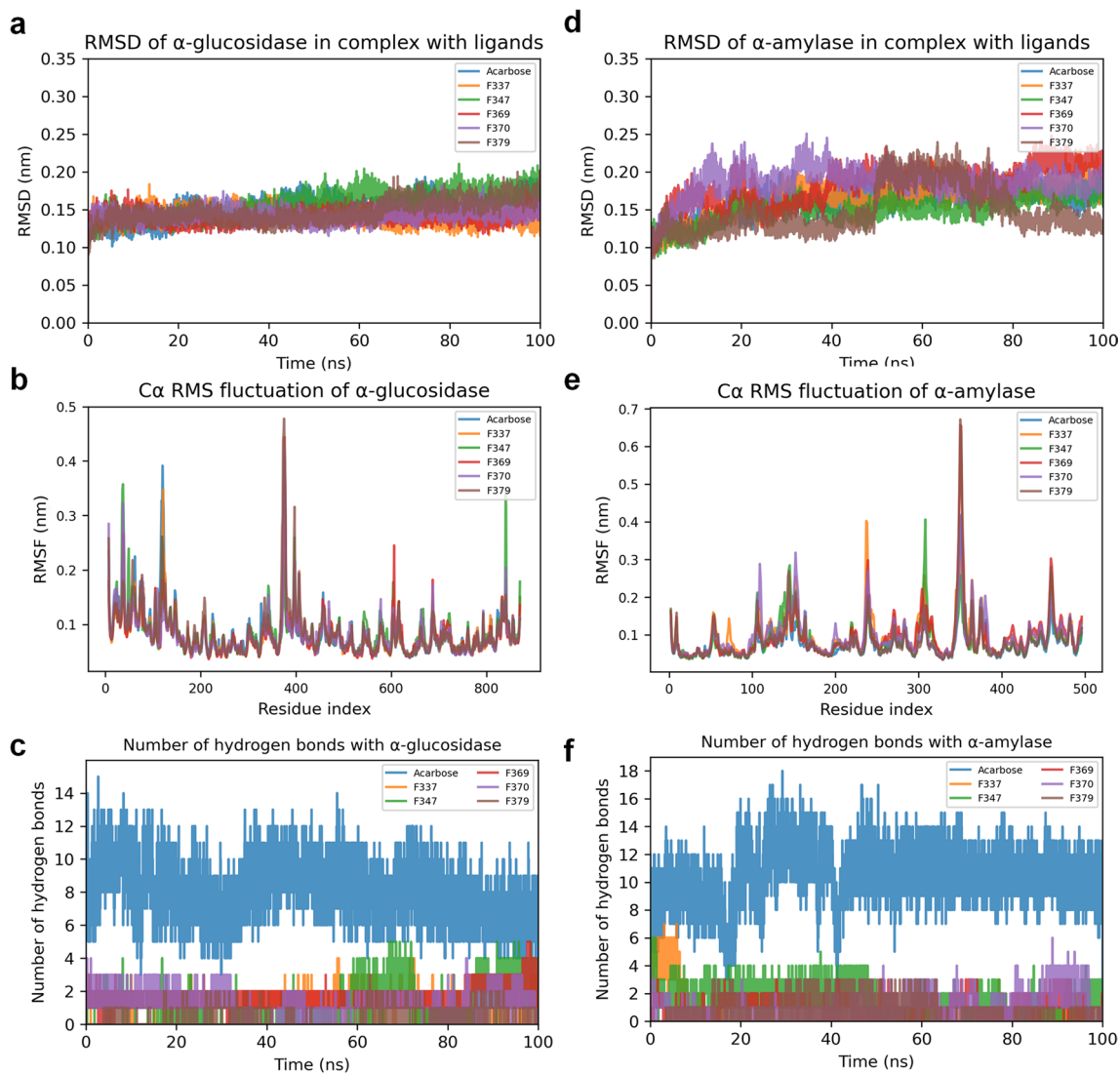


**Fig. 9** Analysis of molecular dynamics simulations using 100 ns trajectories. **a** RMSD value of carbon backbone of  $\alpha$ -glucosidase, **b** RMSF value of C $\alpha$  of  $\alpha$ -glucosidase and **c** the number of hydrogen bonds with  $\alpha$ -glucosidase during the MDS with different ligands; **d**

RMSD value of carbon backbone of  $\alpha$ -amylase, **e** RMSF value of C $\alpha$  of  $\alpha$ -amylase and **f** the number of hydrogen bonds with  $\alpha$ -amylase during the MDS with different ligands

complexes. The detailed RMSD value along the 100 ns duration (Fig. 9 and Fig. S2) also shows that all the complexes could reach equilibrium within the first 1 ns, indicating the high stability of the protein–ligand complexes during the MD simulations. Other interpreting values, such as SASA and  $R_{\text{gyr}}$ , also aligned well with this observation.

In terms of the  $\alpha$ -amylase complexes, although there was an observable variance between the RMSD value of the acarbose–protein complex and that of the compound **F347**, **F369**, **F370**, and **F378**, the detailed value along the MD trajectories, nevertheless, shows the stability of the protein structure, as most of them still could reach equilibrium within 40 ns of MDS (Fig. S2). However, this is not the case for compound **F378**, although have reaching equilibrium in the first 50 ns, the RMSD value skyrocketed to 0.20 nm, before stabilizing back to 0.13 nm in the last 20 ns. This could be explained by the high fluctuation of the loop consisting of Asn350, which is far away from the targeted binding cavity and could be omitted (Fig. 9).

As for hydrogen bonding, it is noteworthy that the number of hydrogen bonds formed between the chalcones and the enzymes remained relatively low compared to the interactions between acarbose and the enzymes. Throughout the simulations, the chalcones were able to form a limited number of hydrogen bonds, ranging from one to six, whereas acarbose exhibited a more substantial number of hydrogen bonds, ranging from five to a maximum of eighteen. This difference can be attributed to the presence of hydroxyl substituents in the acarbose structure.

Despite the lower number of hydrogen bonds, our chalcones demonstrated remarkable inhibitory activity. These findings align with the results obtained from the structure–activity relationship (SAR) analysis and molecular docking, highlighting the significance of hydrophobic interactions between the chalcones and the digestive enzymes. The subsequent section provides a more in-depth analysis of the interactions of flavonoids with the enzymes, shedding further light on their inhibitory mechanisms.

### Stability of investigated flavonoid compounds during the MDS

Regarding the  $\alpha$ -glucosidase simulation, as previously described, because of the shallow nature of the binding cavity of the enzyme, most flavonoids could not penetrate deeply to contact with the catalytic residues. This is also clearly demonstrated in our MDS results (Fig. 10). Apart from the compound **F369**, most of the chalcones underwent transformations during the MD simulations to fit in the binding pocket but could only interact with the gatekeeper residues of the cavity, except for the **F378** ligand. Particularly, this small molecule could not stabilize in the docked binding cavity, as it rotated noticeably around the binding site before

freely moving in the solvation box. This could be explained by the shortage of hydrogen bond donor and acceptor atoms in the structure of the **F378** ligand. Although not being stabled in the anticipated binding pocket, most of our small molecules could outperform acarbose, in terms of their  $IC_{50}$  value against  $\alpha$ -glucosidase. The instability of the ligands during the MDS suggests that the inhibitory mechanism of our investigated ligands toward  $\alpha$ -glucosidase could be via uncompetitive, non-competitive, or a mixed manner. Further discussion is available in the Discussion part.

On the other hand, our chalcones were able to bind consistently to the active site of human pancreatic  $\alpha$ -amylase, revealed by the MDS results. As can be seen in Fig. 11, although the chalcones also needed to undergo some transformations, they managed to stabilize inside the anticipated binding pocket. The binding capability of the chalcones could be explained by the deeper cavity of the enzyme, therefore increasing the possibility of the chalcones interacting with the catalytic residues inside the pocket. The results from our MDS suggest that our chalcones could competitively inhibit  $\alpha$ -amylase. However, further experimental evaluations need to be conducted to confirm the hypothesis.

### Predicted ADMET properties of the top hit compounds

Table S6 contains detailed information on the medicinal chemistry properties, ADME, and toxicity of the five potential dual inhibitors of  $\alpha$ -glucosidase and  $\alpha$ -amylase. Their physicochemical properties are also illustrated in Fig. S3. According to the mechanism of inhibiting the hydrolysis and digestion of polysaccharide chains to treat T2DM, we consider a shortlist of the ADMET properties presented in Table 4. The results predicted by the ADMETlab 2.0 show that these 5 chalcones are accepted by the Lipinski and Golden Triangle rules. A more favorable ADMET profile may be seen in compounds that adhere to the Golden Triangle guideline. All compounds had good oral bioavailability, as indicated by the Human Intestinal Absorption (HIA) probability. They were not P-glycoprotein substrates but may be inhibitors of this transport protein (except for the compound **F337**). The probability of blood–brain barrier penetration from these compounds was also not high (except for the compound **F370**). In addition, these chalcones were predicted to have no acute toxicity. In general, they have no serious cardiovascular toxicity (as predicted by the hERG blockers classification). Four of the five compounds were predicted to be associated with varying degrees of carcinogenicity, but none reached the highest predicted level (+++). This property needs to be considered for optimization in the next stages of drug development. Finally, for the liver, these substances have low predicted human hepatotoxicity and drug-induced liver injury.



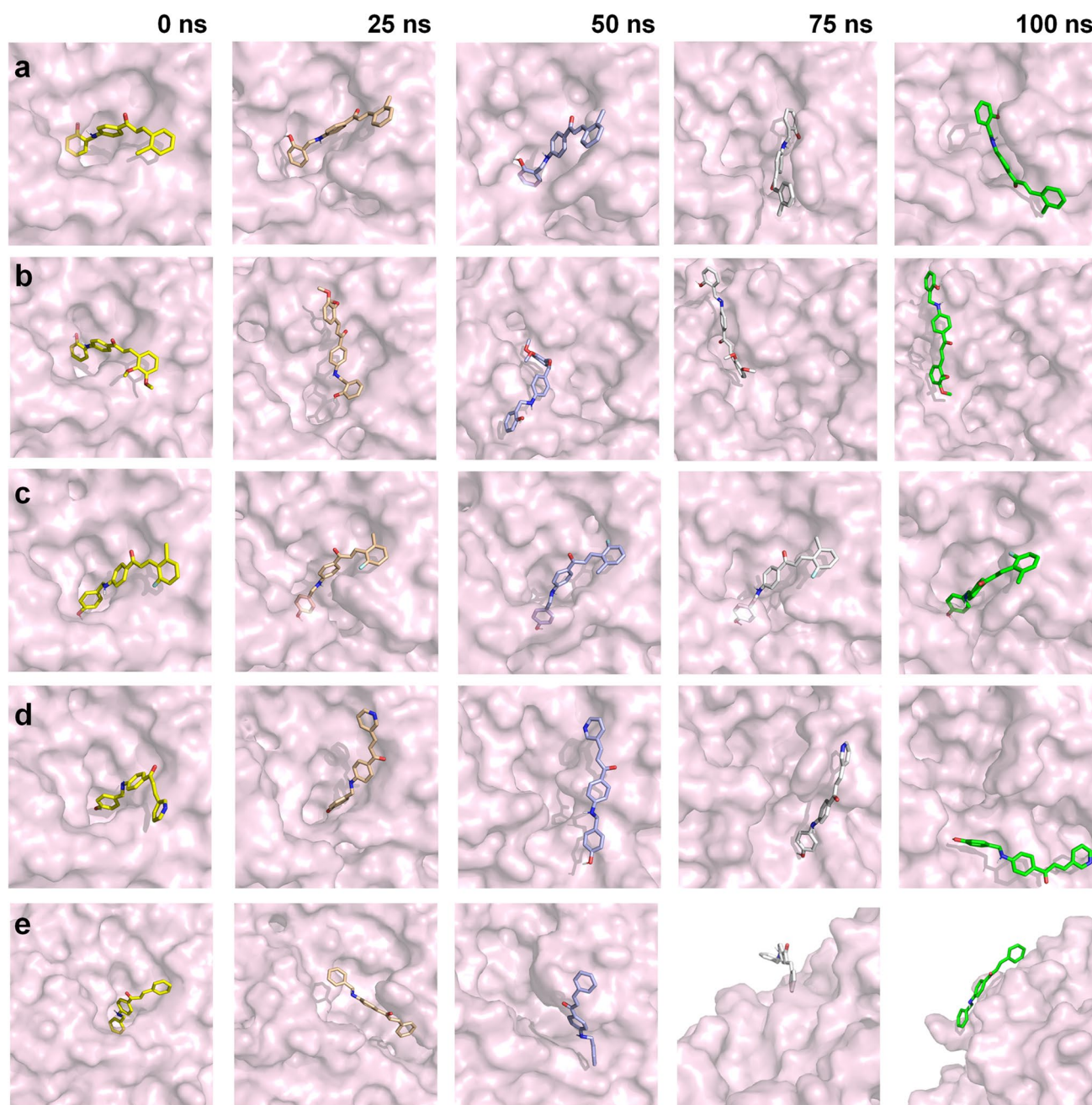


**Fig. 10** Binding conformations of the ligand **a** F337; **b** F347; **c** F369; **d** F370; and **e** F378 with  $\alpha$ -glucosidase. Different ligand colors indicate a different timeframe, with 0 ns (yellow); 25 ns (salmon); 50 ns (blue); 75 ns (white); 100 ns (green)

## Discussion

$\alpha$ -Glucosidase and  $\alpha$ -amylase are two promising targets for the treatment of T2DM. However, currently available therapeutic agents such as acarbose, miglitol, and voglibose are not widely used because of adverse drug reactions. This raises the need for a more effective agent that can simultaneously inhibit  $\alpha$ -glucosidase and  $\alpha$ -amylase for a better sugar blood-maintaining outcome with minimal

side effects. Flavonoids, a ubiquitous naturally occurring class, have long been considered to be active in many systems and have multiple benefits to human health [64–67], therefore they could be a safe and well-tolerated approach for the treatment of T2DM. In this study, by combining both the computational and experimental approaches, we retrieved twelve *N*-benzylaminochalcones that were able to inhibit  $\alpha$ -glucosidase stronger than the commercially available drug acarbose, five of which were able to inhibit

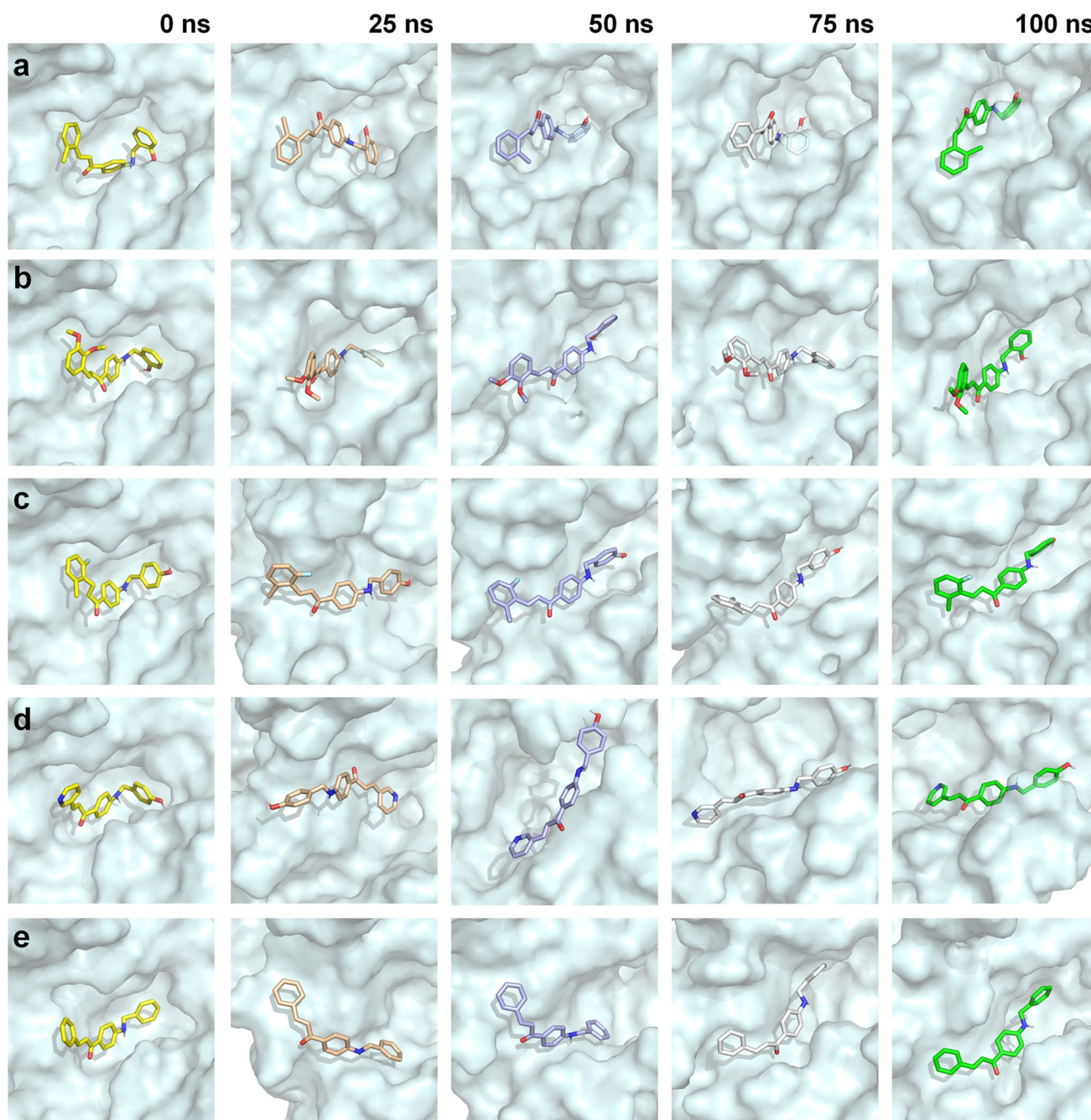


**Fig. 11** Binding conformations of the compound **a** F337; **b** F347; **c** F369; **d** F370; and **e** F378 with  $\alpha$ -amylase. Different ligand colors indicate a different timeframe, with 0 ns (yellow); 25 ns (salmon); 50 ns (blue); 75 ns (white); 100 ns (green)

simultaneously the  $\alpha$ -amylase enzyme, also with a stronger activity than acarbose.

Regarding the  $\alpha$ -glucosidase inhibition, although being able to achieve outstanding *in vitro* results, our MDs results show that most of the compounds were not able to bind stably in the desired binding site. This indicates that our investigated compounds may not inhibit this enzyme via the competitive mechanism. This is not unusual as

multiple research in literature have reported that chalcones may inhibit  $\alpha$ -glucosidase via either competitive [41], non-competitive [36], or mixed-type inhibition [68]. Within the same study, even the introduction of the  $-OH$  group could transit the inhibitory mechanism from uncompetitive to competitive [69]. Therefore, a case-by-case inhibitory mechanism evaluation should be conducted to confirm the hypothesis.

**Table 4** Several important predicted ADMET properties of flavonoid derivatives as potential dual inhibitors against  $\alpha$ -glucosidase and  $\alpha$ -amylase

ADMET properties	Compounds				
	F337	F347	F369	F370	F378
Lipinski	Accepted	Accepted	Accepted	Accepted	Accepted
Golden triangle	Accepted	Accepted	Accepted	Accepted	Accepted
Human intestinal absorption	Excellent	Excellent	Excellent	Excellent	Excellent
P-glycoprotein inhibitor	–	+++	+	+	++
P-glycoprotein substrate	----	----	----	----	----
Blood–brain barrier penetration	--	--	--	+	--
Acute toxicity	0	0	0	0	0
hERG blockers	----	--	–	++	–
Carcinogenicity	+	++	++	--	+
Human hepatotoxicity	--	--	++	–	–
Drug-induced liver injury	–	–	--	–	--

The prediction probability values were transformed into 6 symbols for the classification endpoints: 0–0.1(----), 0.1–0.3(--), 0.3–0.5(–), 0.5–0.7(+), 0.7–0.9(++), and 0.9–1.0(+++) [60]

Concerning  $\alpha$ -amylase inhibition, the stability of the ligands inside the binding cavity of  $\alpha$ -amylase suggests that these compounds could inhibit enzymes competitively. This hypothesis aligns well with the co-crystallized structure of  $\alpha$ -amylase with myricetin (also a flavonoid structure) [23] and the majority of studies in the literature [41, 42, 69].

The discovered chalcones exhibit significant potential as more effective and safer therapeutic agents for the treatment of diabetes mellitus. Their ability to act as multi-target inhibitors, targeting both  $\alpha$ -glucosidase and  $\alpha$ -amylase enzymes simultaneously, provides distinct advantages in managing blood glucose levels. Moreover, some chalcones have shown inhibition of other putative targets for diabetes treatment, such as protein tyrosine phosphatase 1B, aldose reductase, and dipeptidyl peptidase-4 [20]. This multi-target characteristic makes flavonoids strong anti-diabetic agents, even at low concentrations, thus reducing the risk of adverse effects. Additionally, their natural origin and predicted safe ADMET profiles make them attractive alternatives to synthetic drugs. The antioxidant and anti-inflammatory properties of flavonoids further contribute to their potential benefits in diabetes management by reducing oxidative stress and inflammation, both implicated in the pathogenesis of the disease [70]. These findings highlight the unique advantages of the discovered flavonoids in dual-target inhibition and their potential as safer therapeutic agents for the management of diabetes mellitus. Further research and clinical investigations are warranted to fully explore their efficacy, pharmacokinetic properties, and long-term safety in diabetic patients.

It is important to acknowledge the limitations of our current study. The small size of the library, comprising a limited range of flavonoid scaffolds, might explain why all the selected compounds share the same *N*-benzylaminochalcone structure. However, to the best of our knowledge,

these twelve chalcones are being investigated for their anti- $\alpha$ -glucosidase and  $\alpha$ -amylase dual-target inhibition for the first time, making this research a valuable starting point for rational design and synthesis in future studies. Another limitation is that, although several approaches exist to determine the inhibitory kinetics of small molecules toward the two digestive enzymes such as the Lineweaver–Burk plot or NMR spectroscopy, we were unable to conduct these experiments due to limited resources in our laboratory. As an alternative approach, we employed molecular dynamics simulations to gain insights into the molecular mechanisms of these chalcones toward the two enzymes. Nevertheless, follow-up experimental results are needed to confirm the computational findings. Furthermore, although our primary objective was to investigate safer anti- $\alpha$ -glucosidase inhibitors, our study did not assess whether the compounds have fewer adverse effects than acarbose or not. Therefore, further *in vivo* research using animal models will be conducted to evaluate the safety of the discovered compounds.

## Conclusion

In this research, a mini-SAR analysis from the literature has been conducted, the results from which were combined with molecular modeling techniques to yield twelve highly potent  $\alpha$ -glucosidase inhibitors. Most notably, five out of these compounds were able to inhibit simultaneously the  $\alpha$ -amylase enzyme with outstanding  $IC_{50}$  value, compared to acarbose. In addition, MD simulations were conducted to estimate the inhibitory mechanism of the dual-target inhibitors. The results suggest that these compounds could inhibit  $\alpha$ -glucosidase non-competitively while inhibiting  $\alpha$ -amylase competitively. Further evaluation using X-ray crystallization

or Lineweaver Burk plot should be conducted to confirm the hypothesis.

**Supplementary Information** The online version contains supplementary material available at <https://doi.org/10.1007/s11030-023-10680-0>.

**Author contributions** TTM and T-DT contributed to conceptualization; TTM, M-HP, T-TN, and T-V-PN contributed to methodology; TTM, M-HP, T-TT, T-TN, T-PL, and NV-TL contributed to formal analysis and investigation; TTM, T-TT, and M-HP contributed to writing - original draft preparation; TTM, T-PL, and C-VTV contributed to writing - review and editing; T-DT, K-MT, and T-V-PN contributed to funding acquisition; T-DT, K-MT, and C-VTV contributed to resources; T-DT and K-MT contributed to supervision. All authors reviewed the manuscript.

**Funding** This work was supported by the University of Medicine and Pharmacy at Ho Chi Minh City for Thanh-Dao Tran under Grant number 162/2019/HĐ-ĐHYD.

## Declarations

**Conflicts of interest** The authors declare no conflict of interest.

## References

- Sapra A, Vaqar S, Bhandari P (2019) Diabetes Mellitus. In: StatPearls [Internet] (ed). StatPearls Publishing, Treasure Island (FL), pp 1–12
- IDF Diabetes Atlas. Available at <https://www.diabetesatlas.org>. Accessed 30 Dec 2022
- Deshpande AD, Harris-Hayes M, Schootman M (2008) Epidemiology of Diabetes and diabetes-related complications. *Phys Ther* 88:1254–1264. <https://doi.org/10.2522/ptj.20080020>
- ElSayed NA, Aleppo G, Aroda VR, Bannuru RR, Brown FM, Bruemmer D, Collins BS, Hilliard ME, Isaacs D, Johnson EL, Kahan S, Khunti K, Leon J, Lyons SK, Perry ML, Prahalad P, Pratley RE, Seley JJ, Stanton RC, Gabbay RA, and on behalf of the American Diabetes A (2022) Classification and diagnosis of diabetes: standards of care in diabetes—2023. *Diabetes Care* 46:S19–S40. <https://doi.org/10.2337/dc23-S002>
- ElSayed NA, Aleppo G, Aroda VR, Bannuru RR, Brown FM, Bruemmer D, Collins BS, Hilliard ME, Isaacs D, Johnson EL, Kahan S, Khunti K, Leon J, Lyons SK, Perry ML, Prahalad P, Pratley RE, Seley JJ, Stanton RC, Gabbay RA, Association obotAD, (2022) 9. Pharmacologic approaches to glycemic treatment: standards of care in diabetes—2023. *Diabetes Care* 46:S140–S157. <https://doi.org/10.2337/dc23-S009>
- Ghani U (2020) Chapter one - Introduction, rationale and the current clinical status of oral  $\alpha$ -glucosidase inhibitors. In: Ghani U (ed) *Alpha-glucosidase inhibitors*. Elsevier, Amsterdam, pp 1–15
- Gong L, Feng D, Wang T, Ren Y, Liu Y, Wang J (2020) Inhibitors of  $\alpha$ -amylase and  $\alpha$ -glucosidase: potential linkage for whole cereal foods on prevention of hyperglycemia. *Food Sci Nutr* 8:6320–6337. <https://doi.org/10.1002/fsn3.1987>
- Poovitha S, Parani M (2016) In vitro and in vivo  $\alpha$ -amylase and  $\alpha$ -glucosidase inhibiting activities of the protein extracts from two varieties of bitter melon (*Momordica charantia* L.). *BMC Complement Altern Med* 16:185. <https://doi.org/10.1186/s12906-016-1085-1>
- Chiasson J-L, Josse RG, Leiter LA, Mihic M, Nathan DM, Palmason C, Cohen RM, Wolever TM (1996) The effect of acarbose on insulin sensitivity in subjects with impaired glucose tolerance. *Diabetes Care* 19:1190–1193. <https://doi.org/10.2337/diacare.19.11.1190>
- Brayer GD, Luo Y, Withers SG (1995) The structure of human pancreatic  $\alpha$ -amylase at 1.8 Å resolution and comparisons with related enzymes. *Protein Sci* 4:1730–1742. <https://doi.org/10.1002/pro.5560040908>
- Proença C, Ribeiro D, Freitas M, Fernandes E (2022) Flavonoids as potential agents in the management of type 2 diabetes through the modulation of  $\alpha$ -amylase and  $\alpha$ -glucosidase activity: a review. *Crit Rev Food Sci Nutr* 62:3137–3207. <https://doi.org/10.1080/10408398.2020.1862755>
- Li C, Begum A, Numao S, Park KH, Withers SG, Brayer GD (2005) Acarbose rearrangement mechanism implied by the kinetic and structural analysis of human pancreatic  $\alpha$ -amylase in complex with analogues and their elongated counterparts. *Biochemistry* 44:3347–3357. <https://doi.org/10.1021/bi048334e>
- Sim L, Willemsma C, Mohan S, Naim HY, Pinto BM, Rose DR (2010) Structural basis for substrate selectivity in human maltase-glucoamylase and sucrase-isomaltase N-terminal domains. *J Biol Chem* 285:17763–17770. <https://doi.org/10.1074/jbc.M109.078980>
- Sim L, Quezada-Calvillo R, Sterchi EE, Nichols BL, Rose DR (2008) Human intestinal maltase-glucoamylase: crystal structure of the N-terminal catalytic subunit and basis of inhibition and substrate specificity. *J Mol Biol* 375:782–792. <https://doi.org/10.1016/j.jmb.2007.10.069>
- Ren L, Qin X, Cao X, Wang L, Bai F, Bai G, Shen Y (2011) Structural insight into substrate specificity of human intestinal maltase-glucoamylase. *Protein Cell* 2:827–836. <https://doi.org/10.1007/s13238-011-1105-3>
- Le M-T, Trinh D-TT, Ngo T-D, Tran-Nguyen V-K, Nguyen D-N, Hoang T, Nguyen H-M, Do T-G-S, Mai TT, Tran T-D, Thai K-M (2022) Chalcone derivatives as potential inhibitors of P-glycoprotein and NorA: an in silico and in vitro study. *BioMed Res Int* 2022:9982453. <https://doi.org/10.1155/2022/9982453>
- Ashraf J, Mughal EU, Sadiq A, Naeem N, Muhammad SA, Qousain T, Zafar MN, Khan BA, Anees M (2020) Design and synthesis of new flavonols as dual  $\alpha$ -amylase and  $\alpha$ -glucosidase inhibitors: structure-activity relationship, drug-likeness, in vitro and in silico studies. *J Mol Struct* 1218:128458. <https://doi.org/10.1016/j.molstruc.2020.128458>
- Ullah A, Munir S, Badshah SL, Khan N, Ghani L, Poulson BG, Emwas A-H, Jaremko M (2020) Important flavonoids and their role as a therapeutic agent. *Molecules* 25:5243. <https://doi.org/10.3390/molecules25225243>
- Zhu J, Chen C, Zhang B, Huang Q (2020) The inhibitory effects of flavonoids on  $\alpha$ -amylase and  $\alpha$ -glucosidase. *Crit Rev Food Sci Nutr* 60:695–708. <https://doi.org/10.1080/10408398.2018.1548428>
- Mahapatra DK, Asati V, Bharti SK (2015) Chalcones and their therapeutic targets for the management of diabetes: structural and pharmacological perspectives. *Eur J Med Chem* 92:839–865. <https://doi.org/10.1016/j.ejmech.2015.01.051>
- Berman HM, Westbrook J, Feng Z, Gilliland G, Bhat TN, Weissig H, Shindyalov IN, Bourne PE (2000) The protein data bank. *Nucleic Acids Res* 28:235–242. <https://doi.org/10.1093/nar/28.1.235>
- Khoo CM (2017) Diabetes Mellitus treatment. In: Quah SR (ed) *International encyclopedia of public health*, 2nd edn. Academic Press, Oxford, pp 288–293
- Williams LK, Li C, Withers SG, Brayer GD (2012) Order and disorder: differential structural impacts of myricetin and ethyl caffeate on human amylase, an antidiabetic target. *J Med Chem* 55:10177–10186. <https://doi.org/10.1021/jm301273u>
- Lasko TA, Bhagwat JG, Zou KH, Ohno-Machado L (2005) The use of receiver operating characteristic curves in biomedical



- informatics. *J Biomed Inform* 38:404–415. <https://doi.org/10.1016/j.jbi.2005.02.008>
25. Erickson JA, Jalaie M, Robertson DH, Lewis RA, Vieth M (2004) Lessons in molecular recognition: the effects of ligand and protein flexibility on molecular docking accuracy. *J Med Chem* 47:45–55. <https://doi.org/10.1021/jm030209y>
26. Mysinger MM, Carchia M, Irwin JJ, Shoichet BK (2012) Directory of useful decoys, enhanced (DUD-E): better ligands and decoys for better benchmarking. *J Med Chem* 55:6582–6594. <https://doi.org/10.1021/jm300687e>
27. Empeureur-Mot C, Zagury J-F, Montes M (2016) Screening explorer—an interactive tool for the analysis of screening results. *J Chem Inf Model* 56:2281–2286. <https://doi.org/10.1021/acs.jcim.6b00283>
28. Empeureur-mot C, Guillemain H, Latouche A, Zagury J-F, Viallon V, Montes M (2015) Predictiveness curves in virtual screening. *J Cheminform* 7:52. <https://doi.org/10.1186/s13321-015-0100-8>
29. Molecular Operating Environment (MOE) (2022) Version 2022.10. Chemical Computing Group Inc., Montreal
30. O’Boyle NM, Banck M, James CA, Morley C, Vandermeersch T, Hutchison GR (2011) Open babel: an open chemical toolbox. *J Cheminform* 3:33. <https://doi.org/10.1186/1758-2946-3-33>
31. Eberhardt J, Santos-Martins D, Tillack AF, Forli S (2021) AutoDock Vina 1.2.0: new docking methods, expanded force field, and python bindings. *J Chem Inf Model* 61:3891–3898. <https://doi.org/10.1021/acs.jcim.1c00203>
32. Adasme MF, Linnemann KL, Bolz SN, Kaiser F, Salentin S, Haupt VJ, Schroeder M (2021) PLIP 2021: expanding the scope of the protein–ligand interaction profiler to DNA and RNA. *Nucleic Acids Res* 49:W530–W534. <https://doi.org/10.1093/nar/gkab294>
33. Liu M, Yin H, Liu G, Dong J, Qian Z, Miao J (2014) Xanthohumol, a prenylated chalcone from beer hops, acts as an  $\alpha$ -glucosidase inhibitor in vitro. *J Agric Food Chem* 62:5548–5554. <https://doi.org/10.1021/jf500426z>
34. Proença C, Freitas M, Ribeiro D, Oliveira EFT, Sousa JLC, Tomé SM, Ramos MJ, Silva AMS, Fernandes PA, Fernandes E (2017)  $\alpha$ -Glucosidase inhibition by flavonoids: an in vitro and in silico structure–activity relationship study. *J Enzyme Inhib Med Chem* 32:1216–1228. <https://doi.org/10.1080/14756366.2017.1368503>
35. Sun H, Song X, Tao Y, Li M, Yang K, Zheng H, Jin Z, Dodd RH, Pan G, Lu K, Yu P (2018) Synthesis &  $\alpha$ -glucosidase inhibitory & glucose consumption-promoting activities of flavonoid–coumarin hybrids. *Future Med Chem* 10:1055–1066. <https://doi.org/10.4155/fmc-2017-0293>
36. Seo WD, Kim JH, Kang JE, Ryu HW, Curtis-Long MJ, Lee HS, Yang MS, Park KH (2005) Sulfonamide chalcone as a new class of  $\alpha$ -glucosidase inhibitors. *Bioorg Med Chem Lett* 15:5514–5516. <https://doi.org/10.1016/j.bmcl.2005.08.087>
37. Chatsumpun N, Sritularak B, Likhitwitayawuid K (2017) New biflavonoids with  $\alpha$ -glucosidase and pancreatic lipase inhibitory activities from *boesenbergia rotunda*. *Molecules* 22:1862. <https://doi.org/10.3390/molecules22111862>
38. Cheng N, Yi W-B, Wang Q-Q, Peng S-M, Zou X-Q (2014) Synthesis and  $\alpha$ -glucosidase inhibitory activity of chrysin, diosmetin, apigenin, and luteolin derivatives. *Chin Chem Lett* 25:1094–1098. <https://doi.org/10.1016/j.ccl.2014.05.021>
39. Chen Y-G, Li P, Li P, Yan R, Zhang X-Q, Wang Y, Zhang X-T, Ye W-C, Zhang Q-W (2013)  $\alpha$ -Glucosidase inhibitory effect and simultaneous quantification of three major flavonoid glycosides in *microctis folium*. *Molecules* 18:4221–4232. <https://doi.org/10.3390/molecules18044221>
40. Tajudeen Bale A, Mohammed Khan K, Salar U, Chigurupati S, Fasina T, Ali F, Kanwal WA, Taha M, Sekhar Nanda S, Ghufuran M, Perveen S (2018) Chalcones and bis-chalcones: as potential  $\alpha$ -amylase inhibitors; synthesis, in vitro screening, and molecular modelling studies. *Bioorg Chem* 79:179–189. <https://doi.org/10.1016/j.bioorg.2018.05.003>
41. Saleem F, Kanwal KKM, Chigurupati S, Solangi M, Nemala AR, Mushtaq M, Ul-Haq Z, Taha M, Perveen S (2021) Synthesis of azachalcones, their  $\alpha$ -amylase,  $\alpha$ -glucosidase inhibitory activities, kinetics, and molecular docking studies. *Bioorg Chem* 106:104489. <https://doi.org/10.1016/j.bioorg.2020.104489>
42. Sahnoun M, Trabelsi S, Bejar S (2017) Citrus flavonoids collectively dominate the  $\alpha$ -amylase and  $\alpha$ -glucosidase inhibitions. *Biologia* 72:764–773. <https://doi.org/10.1515/biolog-2017-0091>
43. Li K, Yao F, Xue Q, Fan H, Yang L, Li X, Sun L, Liu Y (2018) Inhibitory effects against  $\alpha$ -glucosidase and  $\alpha$ -amylase of the flavonoids-rich extract from *Scutellaria baicalensis* shoots and interpretation of structure–activity relationship of its eight flavonoids by a refined assign-score method. *Chem Cent J* 12:82. <https://doi.org/10.1186/s13065-018-0445-y>
44. Meshram G, Vala V, Wagh P, Deshpande SS (2016) Ultrasound accelerated synthesis of novel benzimidazole derived chalcones as glucosidases inhibitor and antimicrobial agents. *Indian J Chem Sect B* 55:613–623
45. Kiruthiga N, Prabha T, Selvinthanuja C, Srinivasan K, Sivakumar T (2018) Design, synthesis and evaluation of recent flavones as anti-diabetics. *Int J Chem Pharm Anal* 5:1–12
46. Lo Piparo E, Scheib H, Frei N, Williamson G, Grigorov M, Chou CJ (2008) Flavonoids for Controlling starch digestion: structural requirements for inhibiting human  $\alpha$ -amylase. *J Med Chem* 51:3555–3561. <https://doi.org/10.1021/jm800115x>
47. Tran T-D, Nguyen T-C-V, Nguyen N-S, Nguyen D-M, Nguyen T-T-H, Le M-T, Thai K-M (2016) Synthesis of novel chalcones as acetylcholinesterase inhibitors. *Appl Sci* 6:198. <https://doi.org/10.3390/app6070198>
48. Wang Z-W, Wang J-S, Luo J, Kong L-Y (2013)  $\alpha$ -Glucosidase inhibitory triterpenoids from the stem barks of *Uncaria laevigata*. *Fitoterapia* 90:30–37. <https://doi.org/10.1016/j.fitote.2013.07.005>
49. Granados-Guzmán G, Castro-Ríos R, Waksman de Torres N, Salazar-Aranda R (2018) Optimization and validation of a microscale in vitro method to assess  $\alpha$ -glucosidase inhibition activity. *Curr Anal Chem* 14:458–464
50. Kusano R, Ogawa S, Matsuo Y, Tanaka T, Yazaki Y, Kouno I (2011)  $\alpha$ -Amylase and lipase inhibitory activity and structural characterization of acacia bark proanthocyanidins. *J Nat Prod* 74:119–128. <https://doi.org/10.1021/np100372t>
51. Xiao Z, Storms R, Tsang A (2006) A quantitative starch-iodine method for measuring alpha-amylase and glucoamylase activities. *Anal Biochem* 351:146–148. <https://doi.org/10.1016/j.ab.2006.01.036>
52. Ahmed MU, Ibrahim A, Dahiru NJ, Mohammed HS (2020) Alpha amylase inhibitory potential and mode of inhibition of oils from *Allium sativum* (Garlic) and *Allium cepa* (Onion). *Clin Med Insights Endocrinol Diabetes* 13:1179551420963106. <https://doi.org/10.1177/1179551420963106>
53. Abraham MJ, Murtola T, Schulz R, Páll S, Smith JC, Hess B, Lindahl E (2015) GROMACS: high performance molecular simulations through multi-level parallelism from laptops to supercomputers. *SoftwareX* 1–2:19–25. <https://doi.org/10.1016/j.softx.2015.06.001>
54. Mackerell AD Jr, Feig M, Brooks Iii CL (2004) Extending the treatment of backbone energetics in protein force fields: Limitations of gas-phase quantum mechanics in reproducing protein conformational distributions in molecular dynamics simulations. *J Comput Chem* 25:1400–1415. <https://doi.org/10.1002/jcc.20065>
55. Zoete V, Cuendet MA, Grosdidier A, Michielin O (2011) SwissParam: A fast force field generation tool for small organic molecules. *J Comput Chem* 32:2359–2368. <https://doi.org/10.1002/jcc.21816>

56. Bhardwaj VK, Singh R, Sharma J, Rajendran V, Purohit R, Kumar S (2021) Identification of bioactive molecules from tea plant as SARS-CoV-2 main protease inhibitors. *J Biomol Struct Dyn* 39:3449–3458. <https://doi.org/10.1080/07391102.2020.1766572>
57. Humphrey W, Dalke A, Schulten K (1996) VMD: Visual molecular dynamics. *J Mol Graph* 14:33–38. [https://doi.org/10.1016/0263-7855\(96\)00018-5](https://doi.org/10.1016/0263-7855(96)00018-5)
58. Schrödinger LLC., The PyMOL Molecular Graphics System. 2020. 2.0.
59. Guerra F, Siemers M, Mielack C, Bondar A-N (2018) Dynamics of long-distance hydrogen-bond networks in photosystem II. *J Phys Chem B* 122:4625–4641. <https://doi.org/10.1021/acs.jpcc.8b00649>
60. Dong J, Wang N-N, Yao Z-J, Zhang L, Cheng Y, Ouyang D, Lu A-P, Cao D-S (2018) ADMETlab: a platform for systematic ADMET evaluation based on a comprehensively collected ADMET database. *J Cheminform* 10:29. <https://doi.org/10.1186/s13321-018-0283-x>
61. Yadav P, Lal K, Kumar A, Guru SK, Jaglan S, Bhushan S (2017) Green synthesis and anticancer potential of chalcone linked-1,2,3-triazoles. *Eur J Med Chem* 126:944–953. <https://doi.org/10.1016/j.ejmech.2016.11.030>
62. Nasli Esfahani A, Iraj A, Alamir A, Moradi S, Asgari MS, Hosseini S, Mojtavavi S, Nasli-Esfahani E, Faramarzi MA, Bandarian F, Larijani B, Hamedifar H, Hajimiri MH, Mahdavi M (2022) Design and synthesis of phenoxymethylbenzimidazole incorporating different aryl thiazole-triazole acetamide derivatives as  $\alpha$ -glycosidase inhibitors. *Mol Divers* 26:1995–2009. <https://doi.org/10.1007/s11030-021-10310-7>
63. Zawawi NKNA, Taha M, Ahmat N, Ismail NH, Wadood A, Rahim F (2017) Synthesis, molecular docking studies of hybrid benzimidazole as  $\alpha$ -glucosidase inhibitor. *Bioorg Chem* 70:184–191. <https://doi.org/10.1016/j.bioorg.2016.12.009>
64. Halliwell B, Rafter J, Jenner A (2005) Health promotion by flavonoids, tocopherols, tocotrienols, and other phenols: direct or indirect effects? Antioxidant or not? *Am J Clin Nutr* 81:268S–276S. <https://doi.org/10.1093/ajcn/81.1.268S>
65. Fan X, Fan Z, Yang Z, Huang T, Tong Y, Yang D, Mao X, Yang M (2022) Flavonoids-natural gifts to promote health and longevity. *Int J Mol Sci* 23:2176. <https://doi.org/10.3390/ijms23042176>
66. Xu SL, Zhu KY, Bi CW, Yan L, Men SW, Dong TT, Tsim KW (2013) Flavonoids, derived from traditional Chinese medicines, show roles in the differentiation of neurons: possible targets in developing health food products. *Birth Defects Res C Embryo Today* 99:292–299. <https://doi.org/10.1002/bdrc.21054>
67. Lam TP, Tran NVN, Pham LHD, Lai NVT, Dang BTN, Truong NLN, Nguyen-Vo SK, Mai TT, Tran TD (2023) Flavonoids as dual-target inhibitors against  $\alpha$ -glucosidase and  $\alpha$ -amylase: a systematic review of in vitro studies. *J Chem*. <https://doi.org/10.26434/chemrxiv-2023-cdlf8-v3>
68. Ryu HW, Lee BW, Curtis-Long MJ, Jung S, Ryu YB, Lee WS, Park KH (2010) Polyphenols from *Broussonetia papyrifera* displaying potent  $\alpha$ -glucosidase inhibition. *J Agric Food Chem* 58:202–208. <https://doi.org/10.1021/jf903068k>
69. Rocha S, Sousa A, Ribeiro D, Correia CM, Silva VLM, Santos CMM, Silva AMS, Araújo AN, Fernandes E, Freitas M (2019) A study towards drug discovery for the management of type 2 diabetes mellitus through inhibition of the carbohydrate-hydrolyzing enzymes  $\alpha$ -amylase and  $\alpha$ -glucosidase by chalcone derivatives. *Food Funct* 10:5510–5520. <https://doi.org/10.1039/C9FO01298B>
70. Basu S, Debroy R, Kumar H, Singh H, Ramaiah S, Anbarasu A (2023) Bioactive phytochemicals against specific target proteins of *Borrelia recurrentis* responsible for louse-borne relapsing fever: genomics and structural bioinformatics evidence. *Med Vet Entomol* 37:213–218. <https://doi.org/10.1111/mve.12623>

**Publisher's Note** Springer Nature remains neutral with regard to jurisdictional claims in published maps and institutional affiliations.

Springer Nature or its licensor (e.g. a society or other partner) holds exclusive rights to this article under a publishing agreement with the author(s) or other rightsholder(s); author self-archiving of the accepted manuscript version of this article is solely governed by the terms of such publishing agreement and applicable law.

## Authors and Affiliations

Tan Thanh Mai<sup>1</sup>  · Minh-Hoang Phan<sup>1</sup> · Thao Thi Thai<sup>1</sup> · Thua-Phong Lam<sup>1</sup>  · Nghia Vo-Trong Lai<sup>1</sup>  · Thanh-Thao Nguyen<sup>2</sup> · Thuy-Viet-Phuong Nguyen<sup>1</sup> · Cam-Van Thi Vo<sup>1</sup>  · Khắc-Minh Thai<sup>1</sup>  · Thanh-Dao Tran<sup>1</sup> 

✉ Thanh-Dao Tran  
daott@ump.edu.vn

<sup>2</sup> Faculty of Medicine and Pharmacy, Tay Nguyen University, Buon Ma Thuot, Dak Lak 630000, Vietnam

<sup>1</sup> Faculty of Pharmacy, University of Medicine and Pharmacy at Ho Chi Minh City, Ho Chi Minh City 700000, Vietnam